Numerical simulation of heat pipes in different applications

Hussein M. Maghrabie [a], A.G. Olabi [b,c], Abdul Hai Alami [b], Muaz Al Radi [d], Firas Zwayyed [b], Tareq salamah [b], Tabbi Wilberforce [c], Mohammad Ali Abdelkareem [b,e,*]

[a] Department of Mechanical Engineering, Faculty of Engineering, South Valley University, Qena 83521, Egypt
[b] Sustainable Energy & Power Systems Research Centre, RISE, University of Sharjah, P.O. Box 27272, Sharjah, United Arab Emirates
[c] Mechanical Engineering and Design, Aston University, School of Engineering and Applied Science, Aston Triangle, Birmingham, B4 7ET, United Kingdom
[d] Department of Electrical Engineering and Computer Science, Khalifa University, Abu Dhabi, United Arab Emirates
[e] Faculty of Engineering, Minia University, Elminia, Egypt

ARTICLE INFO

Keywords:
Heat pipe
Components and geometry
Applications
Types of heat pipe
Numerical simulation
Thermal performance

ABSTRACT

Nowadays heat pipes are considered to be popular passive heat transfer technologies due to their high thermal performance. The heat pipe is a superior heat transfer apparatus in which latent heat of vaporization is employed to transfer heat for an extended distance under a limited operating temperature difference. Numerical simulation of heat transfer devices is a principal step before implementing in real-life applications as many parameters can be tested in cost-and time-effective behaviors. The present study provides a review of the numerical simulations of various heat pipes in different applications such as cooling of electronic components, heating, ventilation, and air conditioning (HVAC), nuclear reactors, solar energy systems, electric vehicles, waste heat recovery systems, cryogenic, etc. Firstly, this work introduces a background about the main components of heat pipes such as an evacuated tube, wick, and working fluid. The fluid flow and thermal performance characteristics of heat pips are discussed, considering the optimum parameters. Finally, the critical challenges and recommendations for future work encountering the broad application of heat pipes are thoroughly studied.

1. Introduction

The exponential growth in fossil fuel usage resulted in severe environmental impact that is clear in climate change [1,2]. Various strategies are being considered for the reduction of the usage of fossil fuel, such as improving the efficiency of the current energy conversion processes through waste heat recovery [3–5], using efficient energy conversion devices with low or no environmental impacts, such as fuel cells [6–8], and using renewable energy sources that are sustainable with low environmental impacts [9–11]. The rate of heat transfer plays an important role in deciding the efficiency of the energy conversion devices and thus their efficiency [12,13]. Heat pipes (HPs) are the most effective passive thermal devices that have the ability to transfer a huge quantity of heat for long distances via vapor diffusion and latent heat phase-change process [14–16]. The conventional heat pipes (CHPs) that have no moving parts consist mainly of a sealed container/evacuated tube, a wick structure that is partially occupied by a working fluid at liquid/vapor equilibrium [17]. The container of HP is usually divided into three main sections: namely evaporator section in which heat is absorbed from the heat source; the insulated section; and the condenser section in which heat is released to the surrounding environment or heat sink [18,19].

HPs that are known as superconductors operate depending on the fundamentals of high heat transfer during the evaporation process [20]. Heat transfer through HPs is maintained by a phase change of the employed working fluid. The absorbed heat by the evaporator from the heat source is transferred to the working fluid in the liquid phase through wick material. In the evaporator section, the working fluid is transferred into a vapor at the exits of the evaporator due to the increasing vapor pressure, and consequently, the vapor flows into the insulated section to reach the condenser section. The absorbed latent heat gained by the working fluid is released at the condenser to the environment as a result of the difference between the wall temperature. Then the working fluid is returned back to the liquid phase due to the condensation process. Finally, the working fluid is returned to the evaporator through the wick substance by the capillary pumping action, and the process is repeated continuously [21].

Heat pipes (HPs) have many advantages, including reliability, light weight, minimum requirements for maintenance, extensive life span,

---

Nomenclature

h	heat transfer coefficient (W/m^{2}K)
Q	heat flow rate (W)
R_{th}	thermal resistance (K/W)
T	temperature (K)

Greek letters

φ	volume fraction (%)
ε	effectiveness (%)
θ	tilt angle (degree)

Acronyms

AHP	annular heat pipe
BTM	battery thermal management
CFD	Computational Fluid Dynamics
CHP	conventional heat pipe
EVs	electric vehicles
FEM	finite element method
FR	filling ratio
FVM	finite volume method
GHG	greenhouse gasses
HP	Heat pipe
HPHE	heat pipe heat exchanger
HVAC	heating, ventilation, and air conditioning
LHP	loop heat pipe
MCSHP	micro channel separate heat pipe
MHP	Micro/miniature heat pipes
MLHP	Miniature loop heat pipe
MOHP	miniature oscillating heat pipe
NePCMs	nano-enhanced phase change materials
NTU	number of transfer unit
OHP	oscillating heat pipe
PCHP	pre-cooled heat pipe
PCM	phase change material
PHP	pulsating heat pipe
PV	photovoltaic
RHP	rotating heat pipe
SHP	separated heat pipe
TEC	thermoelectric cooler
ULHPs	ultra-thin loop-heat pipes
VCHP	variable conductance heat pipe
VOF	volume of fluid
WHR	waste heat recovery

low cost, and high thermal performance [22,23]. As well, HPs come in various shapes and sizes, each with different properties that have been excessively utilized in various engineering applications [24–29], such as automotive systems [30], nuclear reactors [31,32], solar collectors [33], latent energy storage systems [34,35], electronic cooling [36,37], fuel cells [38], and heating, ventilation, and air conditioning (HVAC) systems [39], etc. Different types of HP are pulsating/oscillating heat pipe (PHP/OHP) [40,41], loop heat pipe (LHP) [42,43], thermosyphon [44], variable conductance heat pipe (VCHP) [45], rotating heat pipe (RHP) [46], annular heat pipe (AHP) [47], sorption heat pipe [48].

The applications of HP are generally grouped into three types: the heat flux transformation in which heat is conveyed from evaporator to condenser; the temperature control in which the system temperature is controlled by heat pipe; and the isothermal applications in which the temperature gradients of pre-existing are reduced. Moreover, heat pipes are also categorized according to their operating temperature ranges into four categories [49]. The first category utilizes the liquid metal for temperatures greater than 700 K, and the second category for temperatures varied from 550 to 700 K by utilizing an organic carbon fluid such as biphenyl. In addition, the third classification is obtained when the temperature is varied from 200 to 500 K by employing ammonia, water, or short carbon organic fluid such as acetone. However, the fourth category can be used when the temperature is less than 200 K by utilizing oxygen, nitrogen, and noble gasses as working fluids.

Numerical simulations of different types of HP for various applications have great attention and necessity in the scientific field with the advancement of technology. A numerical simulation is an effective approach to analyzing different aspects, such as technical or economic of complex systems and applications [50]. Numerical simulations are preferred in terms of cost and time over physical models, particularly for large-scale or material-intensive systems. As well, numerical simulations can eliminate human and instrumental inaccuracies. However, the experimental studies are mandatory to verify the results of the numerical simulations. Generally, from the aforementioned literature review, it can be noticed that most of the available review published works were conducted to study the opportunities and challenges of HPs [24–28], advances in science and technology of HPs [51], RHPs performance [52], characteristics of nanofluids in HPs [53], machine learning methods [54], thermal performance of HP solar collectors [55], working

fluid of PHPs [56], the technology of micro heat pipe (MHP) cooled reactor [57], etc.

As per the authors' knowledge, there is no accomplished work to study the various numerical simulations for different types of HPs. In the present paper, a general background about heat pipes will be presented. As well, different simulation methods for various types and parts of heat pipes for numerous applications and operation modes will be discussed. The current review article introduces different types of HP, such as variable conductance heat pipe (VCHP), thermosyphon heat pipe, loop heat pipe (LHP), pulsating/oscillating heat pipe (PHP/OHP), and others. The numerical simulations are reviewed for different applications of HPs such as electronic components, HVAC, nuclear reactors, solar energy systems, electric vehicles, waste heat recovery systems, cryogenic, etc., and other applications. Additionally, the recommendations for future work encounter the broad application of heat pipes are thoroughly studied.

2. Components of heat pipes

HP is an efficient heat transfer instrument in which the latent heat of evaporation is employed to transform heat for a long distance under a limited temperature difference. The working fluids flow through the wick structure. Heat pipes are broadly utilized for thermal management and waste heat control systems to remove heat to avoid hot spots due to high heat fluxes [58–60].

The casing of HPs is vacuumed at first, then loaded with appropriate working fluid and sealed to separate the working fluid from the ambient environment [18]. Hence, it should allow the heat transfer to/from the working fluid, maintain a pressure difference across the heat pipe walls, and be leak-proof. Selecting the casing of HP depends on a number of parameters such as the thermal conductivity of the material, type of working fluid, ambient environment, weight filling ratio, ease of fabrication, wettability, porosity, etc. The casing should be non-porous with a high thermal conductivity to avoid leakage of vapor and guarantee the required temperature drop between the wick and heat source [21].

On the other hand, the wick's main duty in HP is to transfer the working fluid from the condenser section in a liquid phase by capillary effect/force to the evaporator and distribute it around the heated areas of the evaporator [21,61]. The performance of the wick material

depends on its porosity, thickness, and pore size. Increasing the wick thickness enhances the flow rate of condensate liquid and decreases the flow pressure drop. Furthermore, wick thickness generates the thermal resistance between the inner HP and the surrounding environment. Finer wick pores could improve the capillary effect and hence increase the hydraulic resistance at the same time while the higher porosity acts as a counterbalance to the hydraulic resistance by increasing the liquid permeability [62]. The heat leakage from the condenser to evaporator can also be minimized by increasing the wick porosity [63]. As well, the wettability of the wick and its compatibility with the working fluid should be taken into consideration.

The wick structures are selected according to the heat pipe's design and orientation; they are generally classified into three types: sintered powder, grooved tube, and screen mesh [64]. Sintered powder wick structures can be either mono-porous with a single characteristic pore size or bi-porous that are suitable for anti-gravity applications with vertical orientation as they provide high capillary forces [21,63,65]. In addition, the sintered wicks demonstrate low-temperature gradients and can withstand high heat flux. According to Semenic and Catton [66], thin mono-porous, thin bi-porous wicks, and thick bi-porous wicks are suitable for applications with a heat flux below 300, 600, and 1000 W/cm^2, respectively. Regarding grooved and screen mesh wicks, capillary action is lower than that of sintered wicks; thus, horizontal or gravity-aided heat pipe orientation is preferred [21,67].

Additionally, heat transfer in HP occurs due to the phase change of the employed working fluid between the condenser and evaporator. The operational temperature range of HP lies within the working fluid's triple point with the coexistence of matter in three phases and the critical point with the coexistence of liquid and vapor phases [14,68]. Different heat pipe applications require diverse operating temperature ranges. Thus the selection of the working fluid with suitable thermal properties such as thermal stability and evaporation and condensation processes at the required operating temperature range is a critical issue for ensuring high performance of heat pipe. The parameters that should be considered to determine the most appropriate working fluid for cryogenic applications below −70 °C and/or low-temperature applications of −70 °C and 270 °C are the wall materials, wick compatibility and wettability, good thermal stability, high surface tension, optimum vapor pressure, thermal conductivity and latent heat, vapor and liquid viscosities, and adequate freezing or pour point [69]. The compatibility is the most important factor and should be carefully handled to avoid the chemical reactions of non-condensable gasses that will result in the failure of HP [70].

For high-temperature applications above 1023 °C, the conductivity, melting and boiling points, latent heat, vapor pressure, the material corrosion resistance of the tube against the employed working fluid, and

wettability of the inner tube wall should be concerned [71,72]. Moreover, limiting the operation of HP such as sonic limit, continuum flow limit, viscous, capillary, boiling, and entrainment limits should be taken into consideration [31,73]. The common working fluids for low-temperature applications are ammonia, water, acetone, and organic fluids with a short carbon chain, such as ethanol, whereas alkali metals such as sodium and lithium are appropriate for high-temperature applications [14,74].

3. Simulation of different types of heat pipes

Different types of HPs with different designs have been constructed for different applications [75,76]. HPs can be either as large as 100 m or be built on a micro-scale named micro heat pipes and can be built in different shapes such as conical or rectangular. All HPs have mainly evaporator and condenser sections, adiabatic sections, and wick structures as presented in Fig. 1. This section encloses a brief overview of different heat pipes including the conventional heat pipe, pulsating/oscillating heat pipes, loop heat pipe, other types of heat pipes.

3.1. Conventional heat pipe (CHP)

Mahjoub et al. [78] analyzed the affected parameters on the operation of the conventional heat pipe (CHP) numerically. A benchmark was constructed for studying the effect of changing a single parameter. The steady-state incompressible flow was solved for the cylindrical coordinates in both the HP wick structure and vapor region using FLUENT software. The continuity, Navier-Stokes, and energy equation were introduced for the vapor region and in porous media, and Darcy's law was employed for the momentum equation. The governing equations were solved by applying the SIMPLE algorithm with a collocated grid scheme. The material thermal conductivity of HP, wick porosity, transmitting heat power, and radius and length of heat pipe were studied. The results revealed that increasing the porosity decreased the pressure drop and increased the thermal resistance. As well, the thermal resistance (R_{th}) of HP decreased with increasing the wall thermal conductivity and the radius of HP, while it increased with increasing the wick porosity.

3.2. Pulsating/oscillating heat pipe (PHP/OHP)

Pulsating/oscillating heat pipe (PHP/OHP) consists of a parallel multi-turn evacuated capillary tube fractionally filled with a working fluid. Its length is sectioned into evaporation, condensation, and adiabatic sections [79]. PHPs operate by the pulsating/oscillatory flow of liquid slugs and vapor plugs [80]. The liquid slugs are driven towards
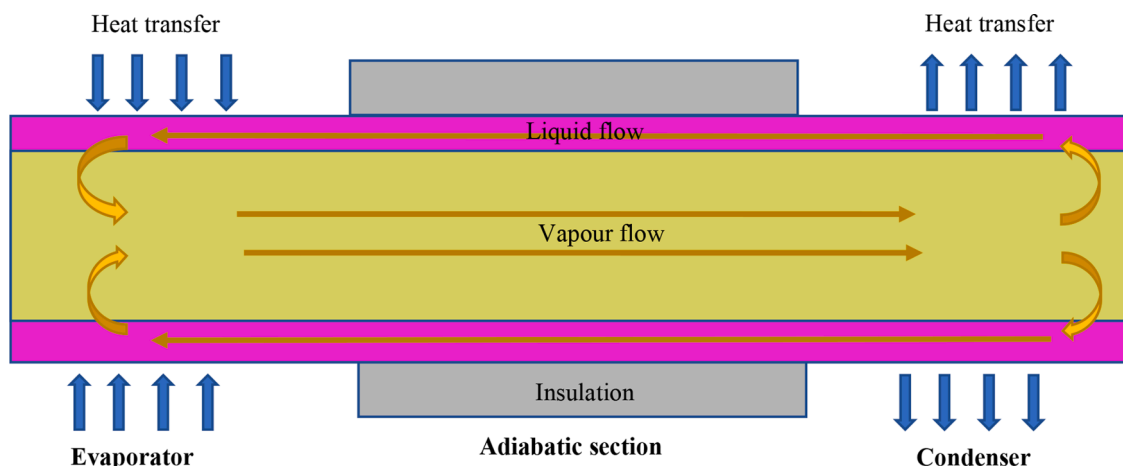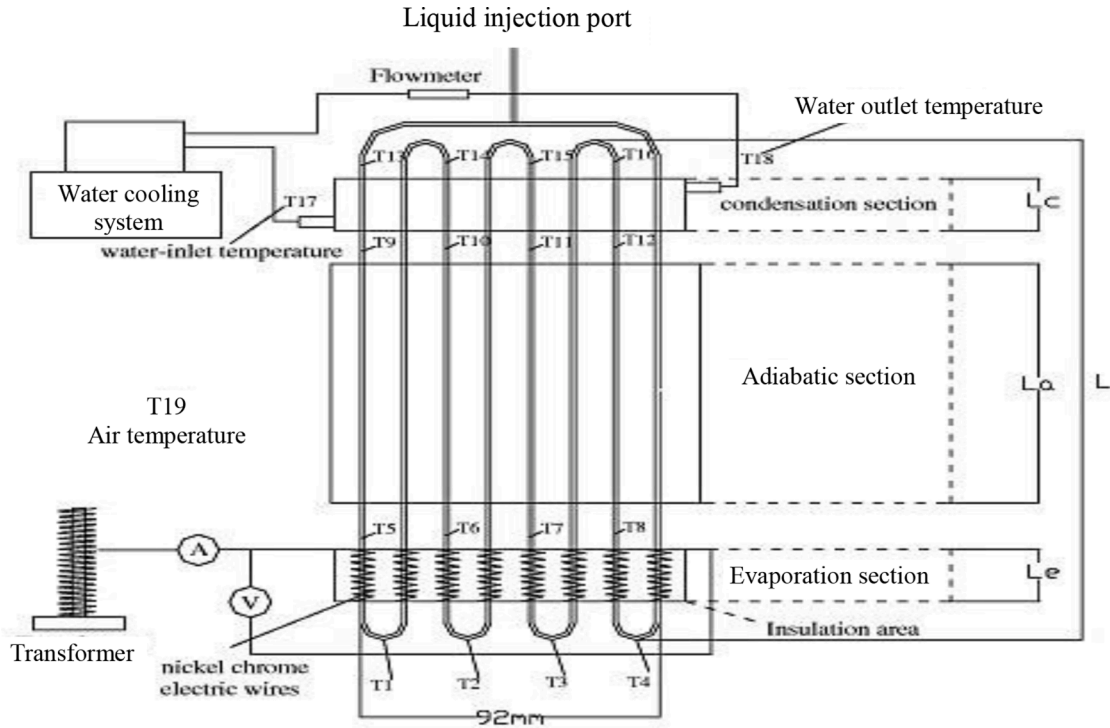

Fig. 1. Fundamental structure of heat pipe [77], reproduced with permission No. 5373,501,465,952.

the condenser by the formation of bubbles inside them, therefore, a wick isn't required in PHPs [81]. There are three main types of PHPs i.e., closed-loop, closed-loop with check valve, and closed-end PHPs [82]. In the closed-loop PHP, heat is transferred by the working fluid due to the pulsation/oscillation effect with a bulk circulation in different directions. In contrast, the closed-loop PHP with check valves enables the fluid to circulate in a certain direction only. The closed-loop PHP is believed by most researchers to be better than other types in terms of heat transfer performance [83,84]. PHPs showed promising performance in the applications of electronic cooling [85], HVAC systems [86], fuel cells [87], hybrid vehicles [88], and solar energy applications [89]. There are a number of advantages of PHP such as simple structure, superior heat transfer capability, low cost, easy system miniaturization, and high flexibility of configuration [90].

Mameli et al. [91] conducted a simulation for a single closed loop PHP to investigate the impact of liquid properties on the simple

Lc: the length of condensation section; La: the length of adiabatic section; Le: the length of evaporation section; L: the heat transfer length of MOHP

(a) Setup for thermal performance test

(b) Semi-visualization experimental setup

Fig. 2. MOHPs apparatus [94], reproduced with permission No. 5373,510,131,434.

geometry. The input parameters were selected to allow the numerical model to work with different working fluids. The Eulerian approach was used for the tube wall control volumes while the fluid control volumes followed the liquid slugs and vapor plugs. Fast Fourier transform (FFT) was conducted on the total liquid momentum to investigate the fluid pressure variation with varying oscillation dominant frequencies. As well, Nekrashevych and Nikolayev [92] conducted a numerical simulation to demonstrate the influence of tube heat conduction on a multi-branch horizontal PHP start-up, operation, and dry-out considering the fluid-tube thermal interaction using the CASCO software. The results demonstrated the impossibility of startup of PHP without bubble generation if tube heat conduction was present. Moreover, the presence of bubble generation prevented the instability of the oscillations that had a large amplitude at long times. Stable oscillations did not start up if the heating power increased the threshold, and the evaporator temperature sharply increased.

Venkata and Bhramara [93] conducted a Computational Fluid Dynamics (CFD) modeling using ANSYS CFX with two-turn PHP using methanol with a filling ratio (FR) of 60%. The boundaries of the condenser, evaporator, and adiabatic section were set for a heat flux in the range of 10–70 W. The hydrodynamics of PHP were characterized by the conservation of mass, energy, and momentum equations. The volume of fluid (VOF) equation was utilized to determine the gas-liquid interface. The simulation results concluded that increasing heat flux decreased the thermal resistance, hence increasing the heat transfer coefficient (h), due to the chaotic movement. As well, 60% FR was more

suitable for PHP operation under a range of heat inputs. In addition, R_{th} of a closed-loop PHP decreased as the heat input increased. Lin et al. [94] introduced a 2D physical model of a miniature oscillating heat pipe (MOHP) using water to simulate the heat transfer of a two-phase flow in a vertical bottom heating mode, as shown in Fig. 2. The simulation considered the temperature change and the oscillating motion due to condensation and evaporation in MOHP. The mixture and the VOF models in FLUENT were used for comparison. The effects of the heat transfer length and inner diameter were analyzed. The c-wall-1 and 2 were employed to record the condensation section's average temperature change. The results indicated that there was a temperature overshoot that demonstrated the bubble generation before reaching the stable oscillation, which complied with the startup characteristics of MOHP. The mixture model was more stable as it kept the temperature oscillation low whereas volume of fluid (VOF) model experienced high-temperature oscillation. Moreover, the results demonstrate that the inner diameter of HP had a considerable influence on the system performance than its length, thus, increasing the inner diameter augmented the thermal performance of MOHP.

Senjaya and Inoue [95] simulated a closed-loop OHP without an adiabatic section and with a bubble generation to discuss the flow behavior of liquid films, liquid slugs, vapor plugs, and heat transfer characteristics. The ideal gas vapor plugs, incompressible liquid slugs, ignoring the turns and gravity effects, constant wall temperature, and constant h and thermal conductivities of vapor plugs, liquid slugs were assumed. 1D mass, momentum, and energy equations were solved in all
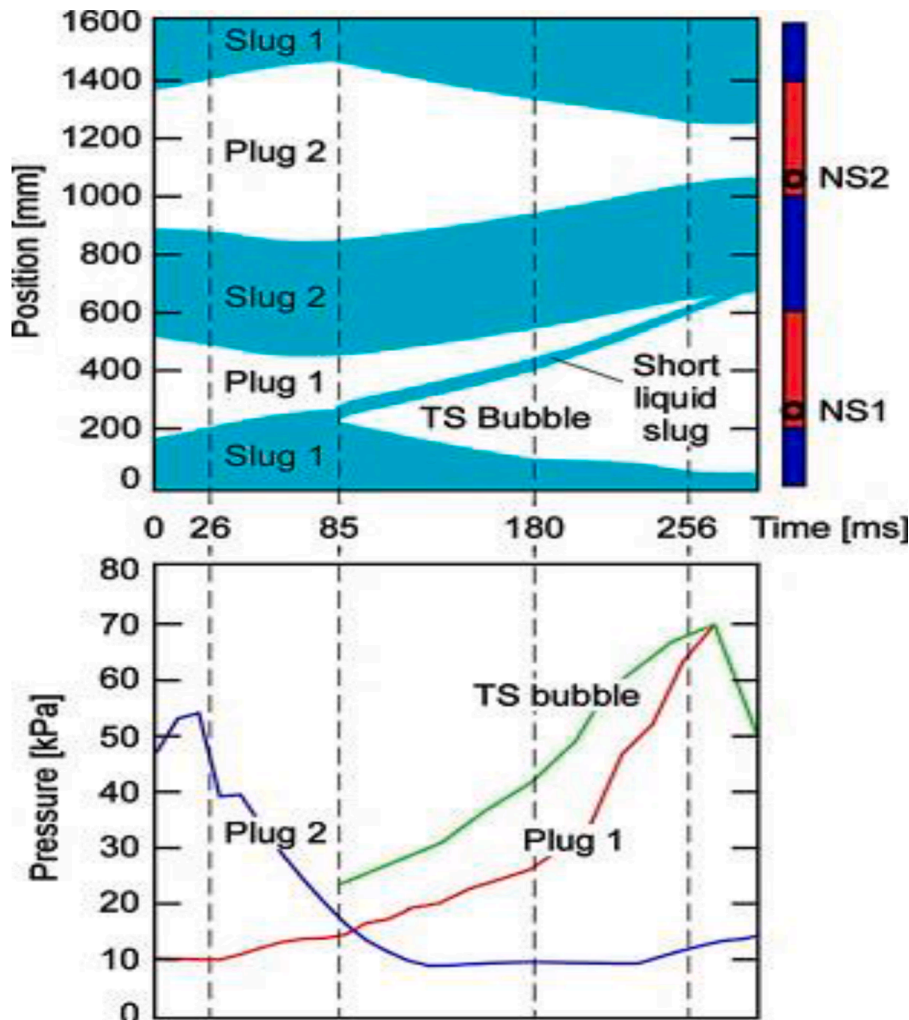

Fig. 3. Simulation results of liquid slugs and vapor plugs [95], reproduced with permission No. 5373,510,299,617.

control volumes using FORTRAN to assess the temperature, velocity, and density of vapor and liquid at each step. The results showed that the continuous growth of bubble generation led to a significant increase in the oscillating frequency, oscillating amplitude, and heat transfer rate. The motion of liquid slugs and vapor plugs became sinusoidal oscillations in the case of bubble generation as presented in Fig. 3. As well, the variation of transferred heat was larger in the case of bubble generation for both latent and sensible heat.

Błasiak et al. [96] Introduced a two-dimensional multiphase flow using a volume of fluid (VOF) method to investigate the performance of a pulsating heat pipe (PHP). The simulation employed a solver for boiling and condensation using a C++ programming language and based on an OpenFOAM-v1612. The simulation was conducted for a working fluid of ethanol using four models of mass transfer with various heat fluxes acting on the PHP. Moreover, the particle image velocimetry (PIV) was used to verify the numerical results of the velocity vector field and the relative error obtained was at a level of 10%.

3.3. Loop heat pipe (LHP)

Loop heat pipe (LHP) known as capillary pump loop (CPL), integrates an evaporator or capillary pump, condenser, liquid and vapor transfer lines/tubes, and a compensation chamber or reservoir [97]. Wicks are only found in the evaporator and compensation chamber which is mostly a fundamental part of the evaporator [98]. The compensation chamber has a number of functions such as storing excess liquid during normal operation and constantly supplying the evaporator's wick with liquid to prevent the dry-out [99]. The primary wick structure of HP or evaporator wick is made up of fine pores in order to create high capillary pressures for the fluid circulation, such as copper powder or sintered nickel with a 55–75% porosity and a pore radius of 0.7–0.15 μm. The secondary wick consists of larger pores to manage the liquid supply from the compensation chamber into the evaporator, particularly when the evaporator is overhead the compensation chamber or in microgravity conditions [100]. The LHPs can be used in the space applications such as the thermal control of space satellites [101], aircraft anti-icing [102], and electronic cooling applications such as tablet PCs and smartphones [103].

Mottet and Prat [104] conducted a numerical model of heat and mass transfer in an evaporator of a loop heat pipe/capillary pumped loop (LHP/CPL) based on a mixed pore network. Two types of wick were studied i.e., monoporous capillary structure and a bidispersed one characterized by a monomodal pore and bimodal pore size distributions, respectively. The pores were distributed with a constant pores and throats size. It was noticed that the throats and pores were distributed randomly. The governing equations were solved by an iterative code written in Fortran 90 and were discretized via the finite volume method (FVM) with grid points centered on pores. The simulation results showed that a positive correlation between the existence of a two-phase zone (liquid-vapor) and the optimum evaporator thermal performance was obtained. Additionally, the thermal performance of the bidispersed wick was lower than that of the monoporous wick at low heat flux, whereas it has a higher heat flux. The monoporous wick caused overheating due to the high presence of vapor in the first pores row beneath the casing
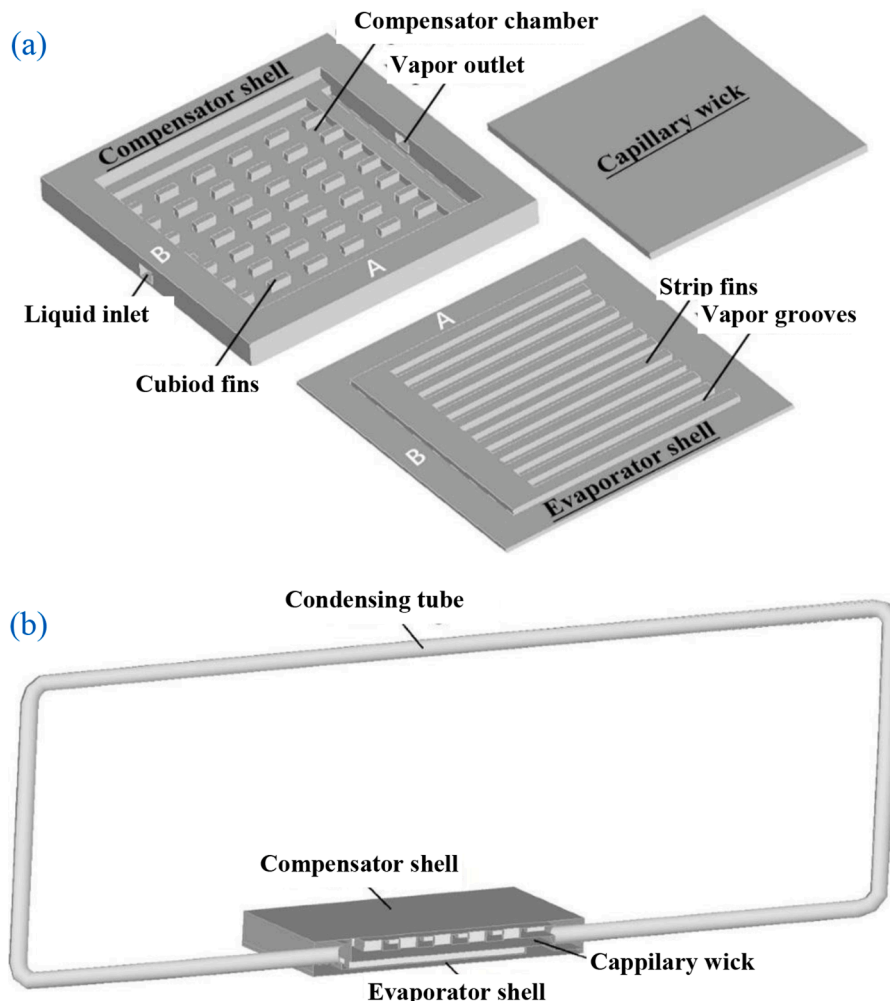

Fig. 4. Proposed LHP (a) separated E-C shells with capillary wick and (b) one-half model of LHP [105].

increasing the thermal resistance. In contrast, a slow increase of casing the overheating occurred in the bidispersed wick as the large pores allowed the vapor to pass and sustain a two-phase zone under the casing.

Zhang et al. [105] carried out a CFD numerical simulation and analysed the reduction of heat leakage in LHP using a capillary wick of carbon fiber using ANSYS software. 3D model and meshing of evaporator-compensator (E-C) and fluid domain were introduced using ICEM CFD. Fig. 4. shows a model of E-C shells and capillary wick and the positions of contact surfaces of E-C shells. The results indicated that the liquid fraction in E-C was almost zero and the heat transfer was reduced for the coated contact surface with yttria-stabilized zirconia (YSZ). Water volume fraction in the compensation chamber was improved from 23 to 37% by the YSZ coating compared to the silicon coating. As well, the addition of copper plating on the carbon fiber wick enhanced the thermal conductivity and the hydrophilic property. The water volume fraction in the compensation chamber was improved from 23% to 98% by the alumina-copper coating and YSZ coating compared to the silicon sheet and copper plating, and the shell temperature of E-C was decreased from 335 to 329.4 K.

Li et al. [106] accomplished a simulation of a pore-scale in a porous wick of a LHP with a flat evaporator via a phase-change Lattice Boltzmann method. The influence of surface wettability and heat flux on the dynamics and patterns of the liquid-vapor interface, temperature variation at the interfaces of wick-fin and wick-groove, liquid volume fraction, and effective h of evaporator were studied. The model was solved by C++ code using openMP parallel algorithm. Different interface patterns of the liquid-vapor i.e., entirely saturated wick (I), partially saturated wick with: periodical nucleation without bubbles (II), periodical growth with the shrink of bubbles (III), the stable interface of liquid-vapor (IV), and fully dry-out at the interface of wick-fin (V) were investigated. In general, the bigger the contact angle and higher the heat flux, the smaller the steady-state liquid volume fraction was maintained. Nevertheless, the liquid volume fraction started oscillating periodically under a specific range of heat flux corresponding to patterns I and II. As the heat flux and contact angle increased, the oscillations' amplitude and period increased. The temperature distributions were asymmetric between the right and left outlets because of the random distribution of pore size in the porous wick. At partially saturated patterns of the interface of liquid-vapor, the inconsistency was significant as shown in Fig. 5 which demonstrates that the local evaporation characteristics are noticeably impacted by the pore structure. As well, the effective h increased as the heat flux raised because of the initiation and growth of bubble nucleation within the wick. The maximum h was accomplished at a lower heat flux for larger contact angles.

Kaya et al. [107] achieved a numerical simulation of the transient operation of LHP to study the overall dynamic nature under vacuum and ambient environments. The numerical model was constructed on the basis of 1D and equations of fluid and heat flow under transient operations using EcosimPro software, and the homogenous model was used for two-phase flow. The governing equations were solved on a staggered grid using a demonstration of the advanced solid-state ladar (DASSL) method. The results concluded that the difficulties regarding the accurate evaluation of evaporator core and grooves conditions were encountered in the case of startup transients at low powers, while startup transients at high powers were successfully reproduced.

Pozhilov et al. [108] conducted a numerical simulation of heat and mass transfer in a 3D model of a satellite LHP evaporator with ammonia as a working fluid. Darcy's law and Reynolds-averaged Navier-Stokes equation were employed to study the flow in vapor and liquid regions, and filtration in the porous structure, respectively. The model was executed in SINF/Flag-S program code and the equations were approximated by a finite volume method (FVM) of the second order of accuracy. Equations of continuity and hydrodynamics were solved using SIMPLEC algorithm. Fig. 6 shows the computational solution domain and the working fluid's flow diagram. The results showed that the evaporation at corners of vapor grooves was the most intense and that the evaporation on the walls of vapor grooves caused the deformation of the vapor velocity profile, hence affecting the pressure drop and friction in the grooves. The maximum heat absorbed by the evaporator was limited when the heat was applied only from the body base. Rising the evaporator wall thickness only slightly reduced the non-uniformity of flow rate distribution in the vapor grooves.

Jung and Boo [109] presented steady-state analytical modeling of LHP coupled with a flat evaporator using a kinetic theory of gasses and thin-film theory. The temperatures and pressures at the evaporator, condenser, liquid reservoir, liquid-transport tube, and vapor-transport tube were studied. The temperature and pressure values were determined for the neighboring zone to the liquid-vapor interface. A mathematical model was built for two types of LHP i.e., with flat evaporator and with cylindrical one. The condenser length was divided into pure-liquid and pure-vapor occupied parts. Effectiveness-number of transfer unit (ε-NTU) method was employed to assess the condenser thermal performance. The results revealed that the amount of heat leakage into the liquid reservoir decreased with increasing the porosity of the capillary structure. It is also observed that a raise in the condenser-outlet temperature can be caused by increasing the vapor-temperature drop inside the condenser, and hence degradation in thermal performance was maintained. Moreover, a reduction in the temperature of the whole evaporate was accomplished by increasing the condenser length.

Nishikawara and Nagano [110] employed a numerical pore network model (PNM) of a capillary evaporator in the LHP with a micro gap
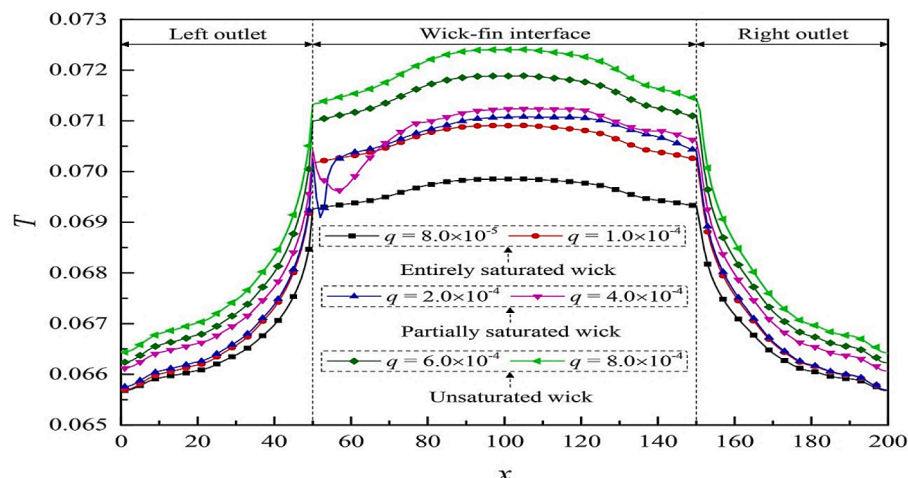

Fig. 5. Temperature variation at the interface of wick-fin and exit in porous wick for different heat fluxes [106], reproduced with permission No. 5373,510,973,565.
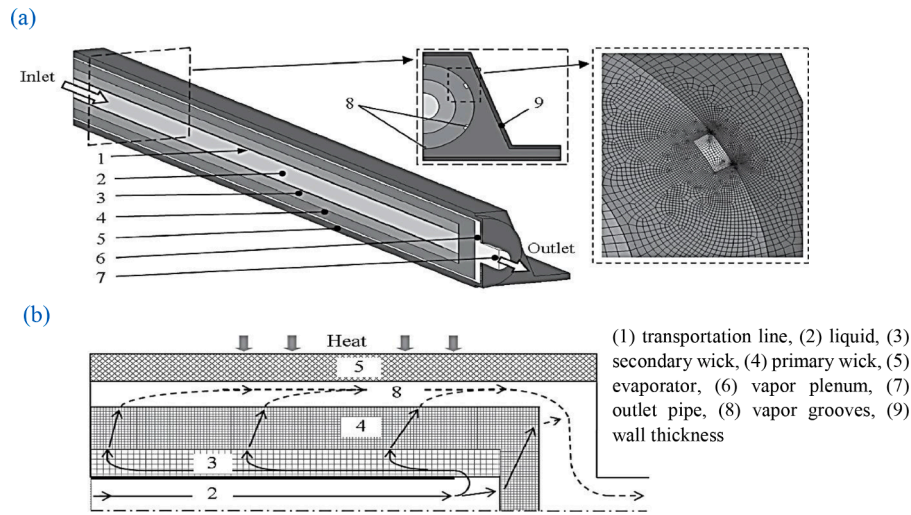
(a)

Inlet

8   9

Outlet

(b)

Heat

5

8

4

3

2

(1) transportation line, (2) liquid, (3) secondary wick, (4) primary wick, (5) evaporator, (6) vapor plenum, (7) outlet pipe, (8) vapor grooves, (9) wall thickness

Fig. 6. Computational solution domain: (a) computational grid and (b) fluid flow diagram [108], open access.

between the HP casing and wick to study the heat transfer characteristics based on standard finite volume methods with cubic lattices mesh size. The results showed that the Nusselt number in the gap fitted to the experimental results was larger than that of the theoretical values of fully developed flow in parallel plates. As well, the h decreased for a small gap distance and continued to decrease as the gap distance increased due to the large saturation temperature distribution. The optimal gap distance of ammonia LHP was smaller than that of ethanol LHP. Additionally, the vapor pocket was hard to exist on the micro gap evaporator for superheating of the liquid in the wick was small.

Zhang et al. [111] developed a 3D model to examine the heat transfer of a miniature LHP using a flat evaporator by a FVM and SIMPLE
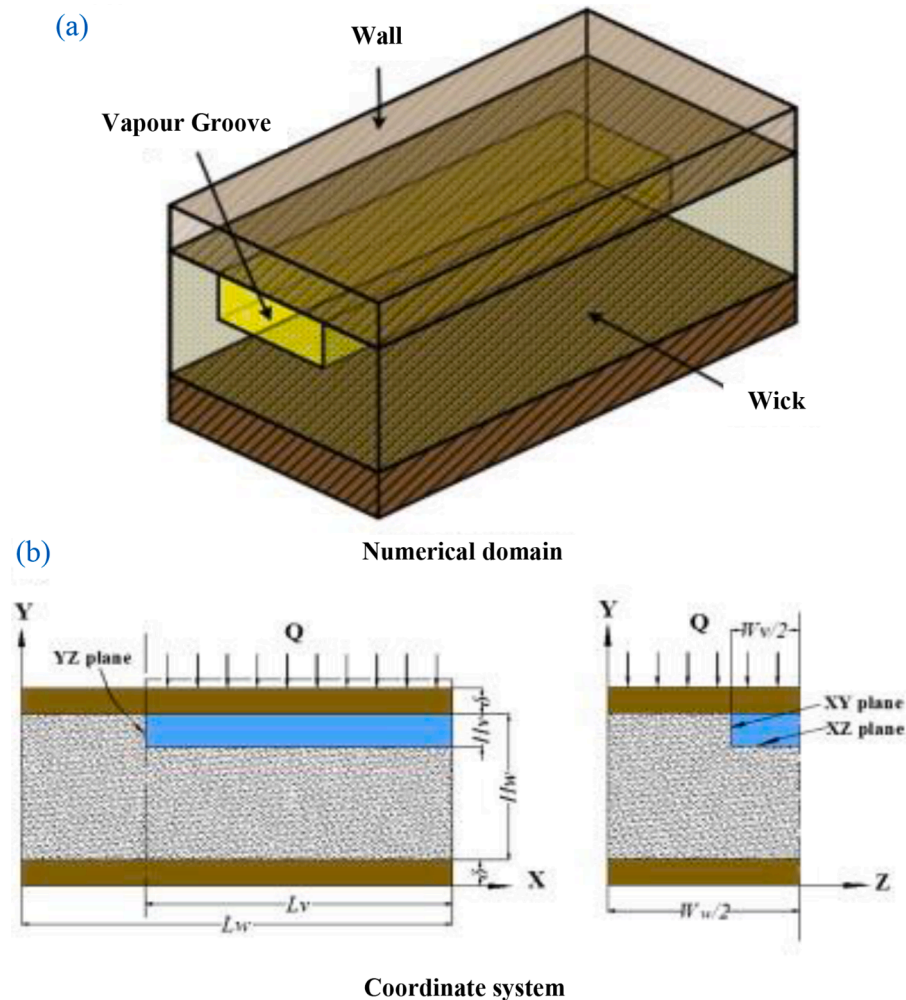

(a)

Wall

Vapour Groove

Wick

Numerical domain

(b)

Coordinate system

Fig. 7. System description: (a) half domain and (b) x-y and z-y planes [111].

algorithm. The heat transfer and fluid flow of wick and the vapor groove integrated by wall heat conduction were considered, as shown in Fig. 7. The boundary conditions of temperature and pressure in combination with the LHP operation were proposed. Impacts of geometrical parameters of vapor groove in a flat evaporator were investigated in detail. The heat load was applied on the top wall of the evaporator for a completely saturated wick with liquid fluid and a fixed liquid-vapor interface between the vapor groove and wick. The results concluded that the h of the evaporator with a vapor groove through wick (I) was higher than for vapor groove inside wall (II) for saturated wick with liquid fluid. In the case I, the optimum form factor (α) defined as the ratio of the height of the vapor groove and its width was unity to achieve the optimal thermal performance. Moreover, when the width ratio of the wick and vapor groove was small, the wick temperature was low.

Chernysheva and Maydanik [112] conducted a numerical simulation to examine the heat and mass transfer transient process of LHP with a cylindrical evaporator during its start-up. The numerical simulation was carried out for various materials of the evaporator and different heat loads. Nickel, copper, and titanium wick were studied for various working fluids i.e., water, ammonia, and acetone. The numerical model consisted of a piecewise uniform grid for spatial coordinate for two subregions i.e., evaporator wall and wick zone of the computational domain. The heat transfer in the evaporator during the start-up was significantly affected by external factors such as the heat load supplied to the evaporator and the conditions of heat transfer between the environment and compensation chamber. The temperature inhomogeneity of evaporator during the start-up process and minimum heat load and time were influenced by the thermophysical properties of the employed working fluid and evaporator materials. A numerical experiment proved that the minimum superheat desired for boiling up of liquid in the vapor removal channels could not be fulfilled for relatively low heat loads which made it impossible to achieve the start-up of the LHP. Therefore, the heat load with minimum value should seriously be considered as one of the major operating parameters of LHP.

Chernysheva and Maydanik [113] presented a 1D model of heat and mass transfer in the evaporator of LHP with an evaporation region combined with vapor-removal grooves in the wick. The results of temperature and pressure distribution were acquired for different working fluids; acetone, ammonia, R141b, and R152a, with varying the evaporator heat flux from 1.8 to 27 W/cm^2. The control volume approach was employed to build a finite difference scheme of the governing equations with appropriate boundary conditions. A nonuniform calculation of the evaporator geometry was employed for a fragment of the evaporator and the Gauss-Seidel iteration approach was utilized to solve a set of linear equations.

3.4. Other types of heat pipes

There are a number of HPs such as variable conductance heat pipe (VCHP), sorption HP, rotating heat pipe (RHP), and annular heat pipe (AHP) that should be considered. VCHP or thermosyphon HP can control the heat flux by attaching a reservoir of inert non-condensable gasses (NCGs) to the condenser. The temperature gradient of HP is a function of heat flux and the condensation area. Thus, the VCHP conductance is controlled by allowing certain amounts of NCGs into the condenser to alter the available condenser area. VCHPs are employed in applications where the reduction or blockage of thermal conductance is required at certain operational modes, mainly in aerospace applications [62, 114]. The variable conductance is a wickless HP that transfers heat exactly the same way as CHPs, where the working fluid flows from the condenser to evaporator via the gravity. Thermosyphons can be implemented for diverse applications such as electronic cooling, waste heat recovery, HVAC systems, and solar collectors, and can achieve significant heat transfer when integrated with heat exchangers [44, 115, 116].

The sorption HP consists of an evaporator and condenser on one end and a sorbent bed including a desorber/adsorber and evaporator at another end. The sorption HPs combine the sorption process of a sorbent bed with the advantages of heat pipe technology [117]. However, in RHP, the working fluid flows from the condenser towards the evaporator via a centrifugal force generated by the rotation of HP [118]. On the other hand, AHP has an annular cross-section of HP instead of a circular one, which allows the wick structure to be placed on the inside and outside of outer and inner pipes, respectively. Hence, the capillary limit is greater than that of a CHP with similar outer dimensions [51].

Arat et al. [119] investigated the thermal performance of glass and copper two-phase closed thermosyphons using a 3D numerical model and experimental implementation based on the Volume of Fluid model and Eulerian model. The two-phase closed thermosyphons were designed as a circular closed tube system with single or two-phase flow heat transfer mechanisms to study the boiling, evaporation, and condensation processes. The results revealed that the boiling process was conducted as the core bubbles and vapor slug up to 25th second. Then, the boiling process was slowed down, while the geyser boiling was accomplished by pulsating at the 40th second.

Ling et al. [120] conducted a simulation model based on Matlab R2016b of a microchannel separate heat pipe (MCSHP) with low heat and mass flux, as illustrated in Fig. 8. A Nusselt laminar liquid condensation theory and ε-NTU method were used to construct the distributed-parameter model. Different heat transfer correlations for two-phase were analyzed using different filling ratios (FRs). The finite element method (FEM) was employed to model the evaporator of MCSHP, and the ε-NTU method was utilized to calculate the cooling capacity of each segment. Moreover, the influences of refrigerant filling ratio, height difference, and air flow rate on the MCSHP performance were investigated. The refrigerant side h in the evaporator and condenser sections was maximum at a FR of 82%. Further, the overall cooling capacity was enhanced by increasing the air flow rate until a certain limit then the effect fades, and fan energy consumption were increased.

Yue et al. [121] conducted a computational simulation on the fluid flow characteristics and heat transfer behavior of a MCSHP employing R22 working fluid with various FRs for special indoor environment cooling. A simplified model of louvered fins on the external surface of HP was used to minimize the computation time without neglecting its heat transfer augmentation. The influence of different FRs on flow patterns, cooling capacity, and thermal characteristics of the MCSHP were studied. A user-defined function was introduced to simulate the condensation and evaporation processes. VOF method of ANSYS FLUENT was utilized to simulate a two-phase flow and motion at the interfaces of MCSHP. The examined HP was designed for multiple immiscible working fluids considering the location of the interface between the working fluids. The observed flow patterns were bubble and slug flows. The cooling capacity, wall temperature distribution and outlet temperature were evaluated. The optimum filling ratio was detected at around 68– 100%. As well, the maximum value of cooling capacity at 4087 W was achieved at a FR of 78%. Increasing the FR increased the liquid fraction, which had a favorable impact on the cooling capacity due to increasing the flooded surface area of the evaporator by two-phase fluid of refrigerant.

Li et al. [122] investigated the boiling-condensation heat transfer in ultrathin flat heat pipes with an enclosed space of 1 mm and anhydrous ethanol using visualization experiments via a high-speed camera and numerical simulation analysis. The enclosed space was vertically oriented with a bottom heating section and a top cooling section. The results demonstrated that the boiling-condensation heat released inside the enclosed space was changed periodically due to the bursting and growth of bubbles and falling of the working medium due to gravity.

Kuang et al. [123] conducted a simulation of the flow behavior of ammonia boiling in an evaporator of a SHP with low heat flux to demonstrate two-phase characteristics. The VOF was used to study the interface between liquid ammonia and gas. In addition, the flow patterns in the evaporation section were studied. Pressure-implicit with the
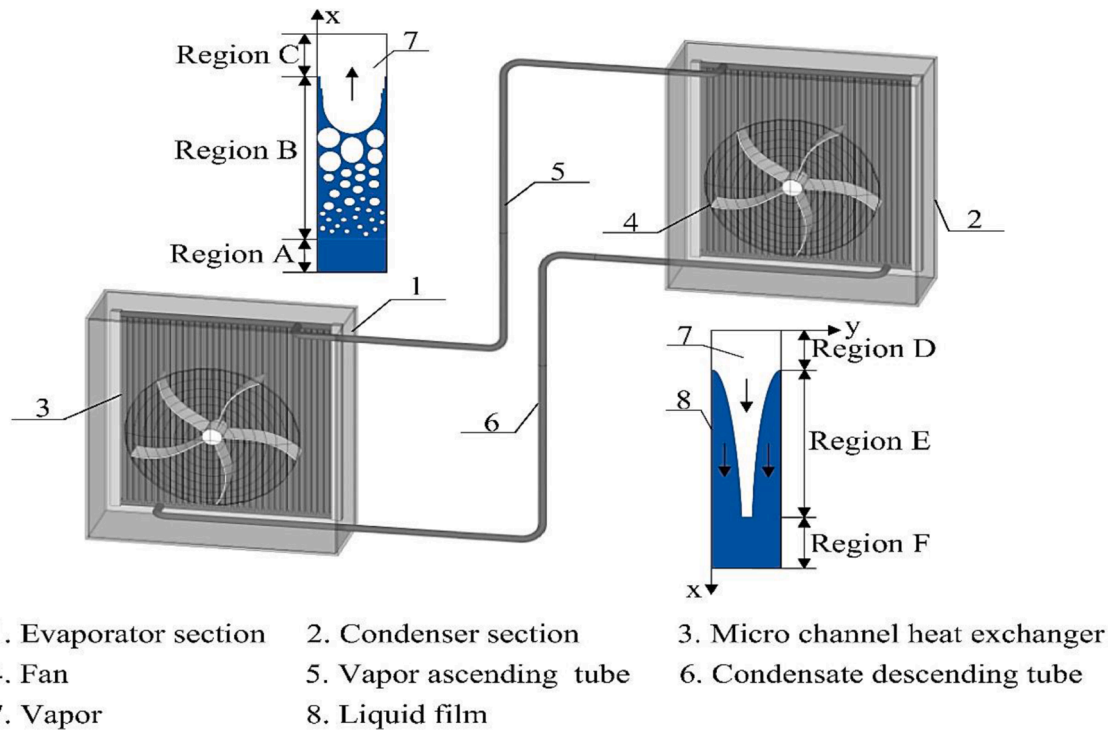
1. Evaporator section   2. Condenser section   3. Micro channel heat exchanger
4. Fan   5. Vapor ascending tube   6. Condensate descending tube
7. Vapor   8. Liquid film

Fig. 8. Schematic of MCSHP including the evaporator and condenser sections [120], reproduced with permission No. 5373,511,414,268.
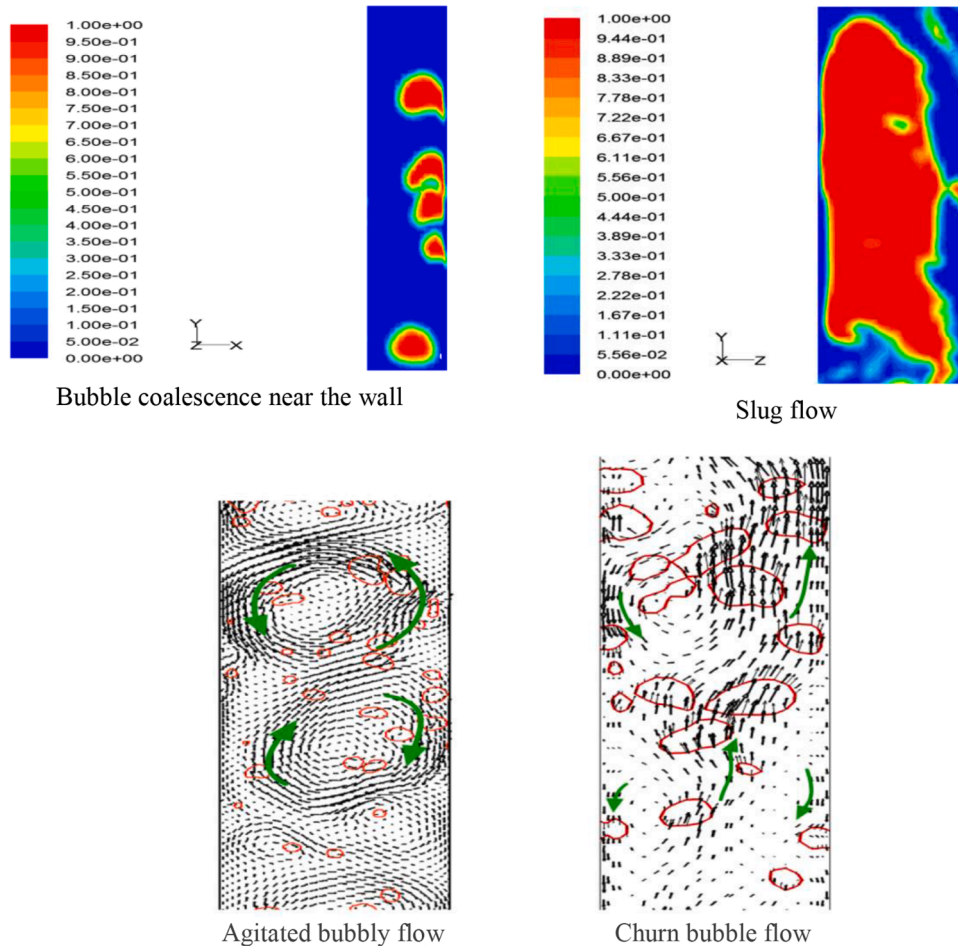

Fig. 9. Flow patterns in heat pipe [123], reproduced with permission No. 5373,520,317,954.

splitting of operators (PISO) was employed for integrating pressure and velocity, along with neighbor correlation and skewness correlation. The model efficiently simulated the flow pattern evolution and was able to properly capture the hydrodynamic and thermal mechanisms, and bubbly and slug flow was noticed. The slug flow was accomplished as a result of the bubbles growth and its consecutive coalescence in the HP. Different behaviors of two-phase flow were noticed for a 65-mm diameter of HP than those of a conventional less diameter pipe. It was observed from the simulation that the churn and agitated bubbly flow occurred along with the formulation of unstable bubble that can break up into churn froth flow as shown in Fig. 9. Nucleate boiling was noticed as a predominant mechanism under the conditions of low mass and heat flux, and the h was low sensitive to mass flux.

Yao et al. [124] established a numerical model of condensation and evaporation processes of an axial grooved heat pipe (AGHP) under a small inclination angle to study the evaporation regimes and the characteristics of heat transfer. The effects of inclination angle and groove structure on the maximum heat transfer were discussed. The numerical simulations indicated that increasing the input power transmitted the fin-film evaporation regime to the corner-film evaporation. Increasing the inclination angle of HP improved the gravitational effect on the liquid reflux and enhanced the critical input power for the evaporation transition regime.

Mashaei et al. [125] accomplished a numerical simulation using FORTRAN to investigate the impacts of aqueous Al_2O_3 nanofluid on the hydrothermal performance of a horizontal mesh cylindrical HP with multiple heat sources of evaporators as shown in Fig. 10. The effects of nanoparticle volume fraction (φ) varied from 0 to 7.5% and the heat load (Q) changed from 14 to 112 W on the velocity and temperature fields, and pressure drop of HP was analyzed. The results indicated a more uniform temperature if the evaporate with a high heat load was placed close to the condenser. Thus, the heat load of the second evaporator (Q_{e2}) was considered 1.33 times higher than that of the first evaporator (Q_{e1}). The power law was implemented to discrete the momentum and energy equations and the pressure and velocity fields using a SIMPLE procedure, and the tridiagonal matrix algorithm (TDMA) was selected to solve the discretized equations. The results revealed that using the nanofluid decreased the velocity in the axial direction for the wick structure as well as enhanced the thermal performance. Whereas increasing the volume concentration increased the pressure drop through the wick. Both pressure drop increment and R_{th} reduction of nanofluid utilization became more significant by decreasing the nanoparticle diameter and increasing the porosity of the wick structure. The

optimum thermal and hydraulic performance due to using Al_2O_3 nanoparticles in HP with discrete heat sources was observed at the nanoparticle concentration of 5% and at the highest value of heat load.

Pooyoo et al. [126] conducted a 3D numerical simulation of a copper cylindrical HP for a laminar steady-state flow and ideal incompressible gas flow in the evaporator section. Non-Darcian transport for the liquid flow through wick and mass flow rate at the interface of vapor-liquid to estimate the velocity, pressure, and temperature profiles were considered. Navier–Stokes, enthalpy, and continuity equations were the governing equations. FVM was utilized to discretize the governing equations to obtain algebraic equations based on the iterative segregated method as well as the algorithm of Simi-Implicit Method Pressure Link Equation-Consistent (SIMPLEC). This model demonstrated the centerline velocity magnitude, centerline pressure, axial outer wall temperature, and thermal performance of cylindrical HP in circumferential heat. The hypotheses were tested by the two-sample method for the outer wall temperature in the axial direction between the present and previous results at 99.5% of confidence and 0.01 at the significance level.

4. Simulation of heat pipes in different applications

The addition of HPs for diverse engineering applications has been expanded to the power systems and industry to secure elevated thermal performance and reduce environmental pollution emissions' influence. Simulating the heat pipes is a critical issue and depends on several operating and design parameters. Additionally, the simulation of HPs for applications such as electronic components, HVAC, nuclear reactors, solar energy, and further applications is reviewed.

4.1. Electronic components

Electronic components are widely employed around the world in various applications such as instruments, computers, cellphones, etc. The advances of electronic components make their operating process faster. So, the performance enhancement in electronic components is engaged with dissipating efficiently the generated heat with a minimum size [127–130]. Optimizing the surface temperature of electronic components due to high heat flux is the main challenge. Li et al. [131] accomplished a numerical simulation on water/ copper micro/miniature heat pipe (mHP) under high power LED multi-chip. Icepak software was used to develop a finite volume model in three-dimension to analyze the temperature distribution. Natural convection, steady-state operation, incompressible and laminar flow, and aluminum heat sink parts
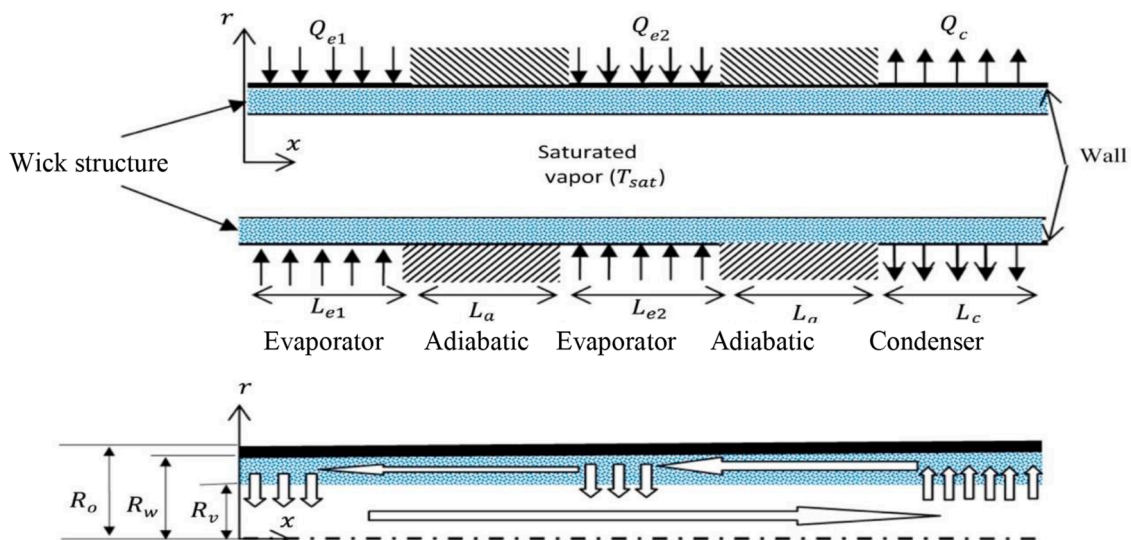

Fig. 10. A cylindrical heat pipe with two evaporators [125], reproduced with permission No. 5374,560,800,428.

were considered. Chips, solder balls, and substrate were modeled as blocks. Unstructured mesh, as well as non-conformal meshing between assembly and background, were used to mesh the model. The influences of the number, thickness, and height of the fins on the performance of the mHP were investigated. The design of the experiment (DOE) was used to select the optimal scheme of heat dissipation by predicting the optimization level of the mentioned factors. The results demonstrated that the source temperature was below 70 °C in natural convection which fulfilled the condition of LED working temperature below 120 °C.

Zhu and Yu [132] simulated the working of an ejector-assisted loop heat pipe (ELHP) under steady-state with a flat evaporator for cooling electronic components, as illustrated in Fig. 11. The ejector eliminated the requirement of subcooling liquid delivered to the compensation chamber to intensify the performance of LHP. As well, it was used to discharge the produced vapor from the compensation chamber due to the heat leaks through the wick. The thermodynamic properties of employed water were calculated using the NIST database. The simulation results were compared with the basic loop heat pipe (BLHP) with a flat evaporator. The influences of total condenser length, wick thickness, diameter line of vapor, water mass flow rate, and the inlet temperature of cooling water on the EHLP's performance were considered. The results showed that, compared with the BLHP, the EHLP achieved a low operating temperature for a short condenser length. As well, EHLP under a low mass flow rate condition maintained a shorter condensor length than the BLHP and it also improved the condenser length even when the diameter of the vapor line was the same as that of the BLHP.

Elnaggar et al. [133] conducted an experimental implementation and simulation based on the finite element method (FEM) of ANSYS to assess the performance of a finned U-shape HP used for cooling a PC. Four U-shaped finned heat pipes were oriented vertically with a heat source that was fixed inside a wind tunnel as shown in Fig. 12. The h and the total thermal resistance ($R_{th,t}$) were evaluated for forced and natural convection modes at steady-state conditions, by changing the air velocity from 1 to 4 m/s, and the heat input from 4 to 24 W. The results indicated that the performance of finned HPs was significantly affected

by the power input and the air velocity. The lowest thermal resistance (R_{th}) of 0.181 °C/W was obtained at 24 W heat input and 3 m/s air velocity while it was 0.441 °C/W for natural convection.

4.2. Heating, ventilation, and air conditioning systems

HVAC systems are introduced to fulfill specified requirements such as comfortable, ensuring healthy, and maintaining safe environmental circumstances for various applications in non-residential buildings [134]. The utilization of a heat pipe heat exchanger (HPHE) is endorsed to minimize the electrical power consumption of HVAC [135]. Yu and Wang [136] proposed a dual-mode control system integrated with a solid sorption HP with an air cooling methodology for the cooling of internet data centers (DC). They constructed 3D calculation models to investigate the temperature and flow distributions for rack level and DC room level. The modeling was based on the Navier-Stokes equations and was performed using CFD analysis SolidWorks. The fluid flows were assumed to be compressible, Newtonian, and steady fluid. Fig. 13 shows a diagram of a solid sorption HP unit combined with a thermal control method for rack level cooling with a maximum allowed temperature for chip operation of 80 °C, using NaBr as a sorbent for the solid sorption HP. The simulation results demonstrated that the flow velocity was relatively high in the air supply regions and return and a considerable velocity gradient was maintained along with the flow direction in the plenum area. In addition, each server's temperature decreased evenly with a specific degree of gradient. The thermal control system decreased the maximum temperature from 75.8 to 68.8 °C. Applying this novel system with a heat load of 1000 W saved approximately 1,741 MWh annually for an HVAC system during the winter seasons.

Ahmadzadehtalatapeh and Yau [137] conducted a full-year model simulation to study the HPHEs with four, six, and eight rows to enhance the air quality and minimize the power consumption of the AC system in Malaysia. The performance of HPHE was evaluated using FORTRAN and TRNSYS that was used to examine the hour-by-hour performance combined AC/HPHX system. The results revealed that the eight-row HPHE
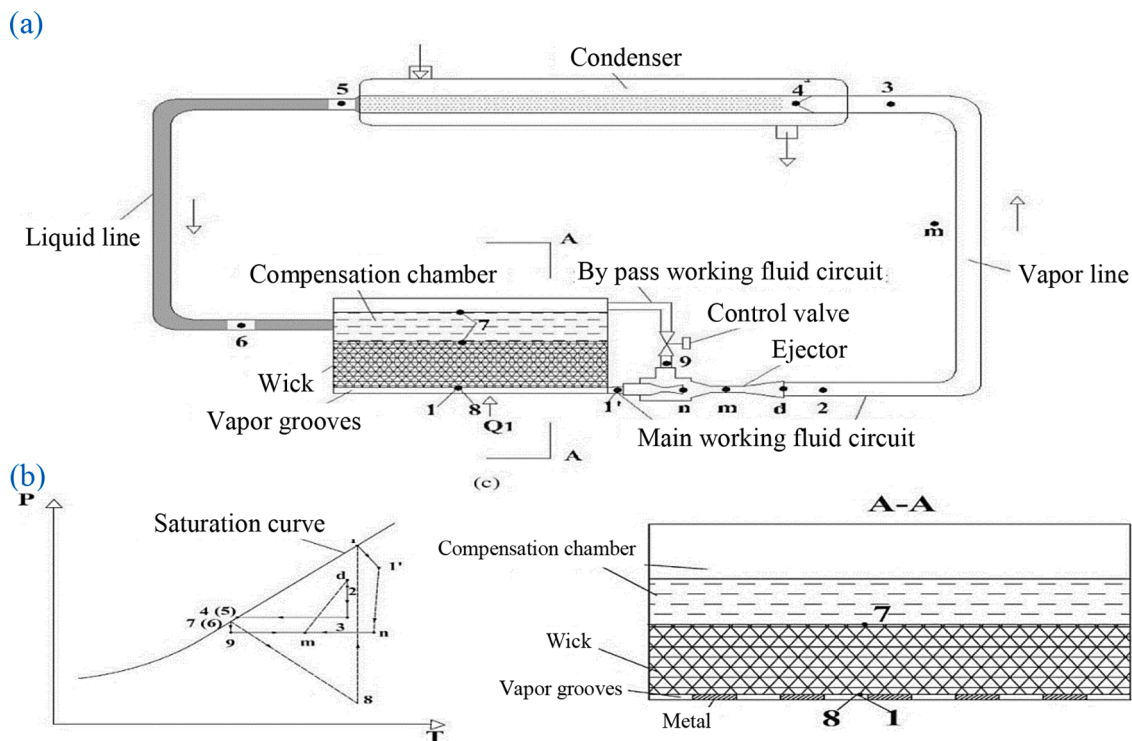

Fig. 11. (a) Schematic of a ELHP (b) pressure–temperature diagram and (c) descriptive structure of different components [132], *reproduced with permission No.* 5373, 520,463,498.
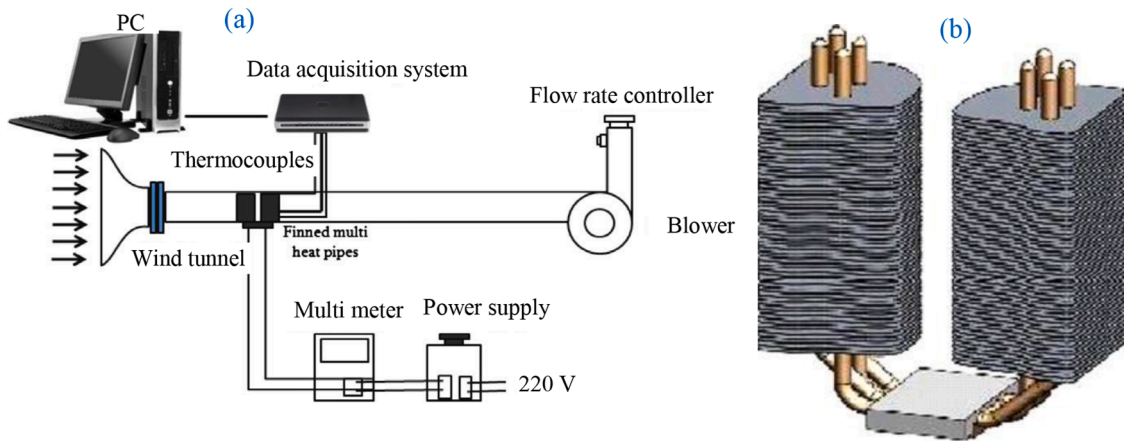
Fig. 12. (a) Experimental setup (b) finned U-shape multi HP [133], reproduced with permission No. 5373,520,571,048.
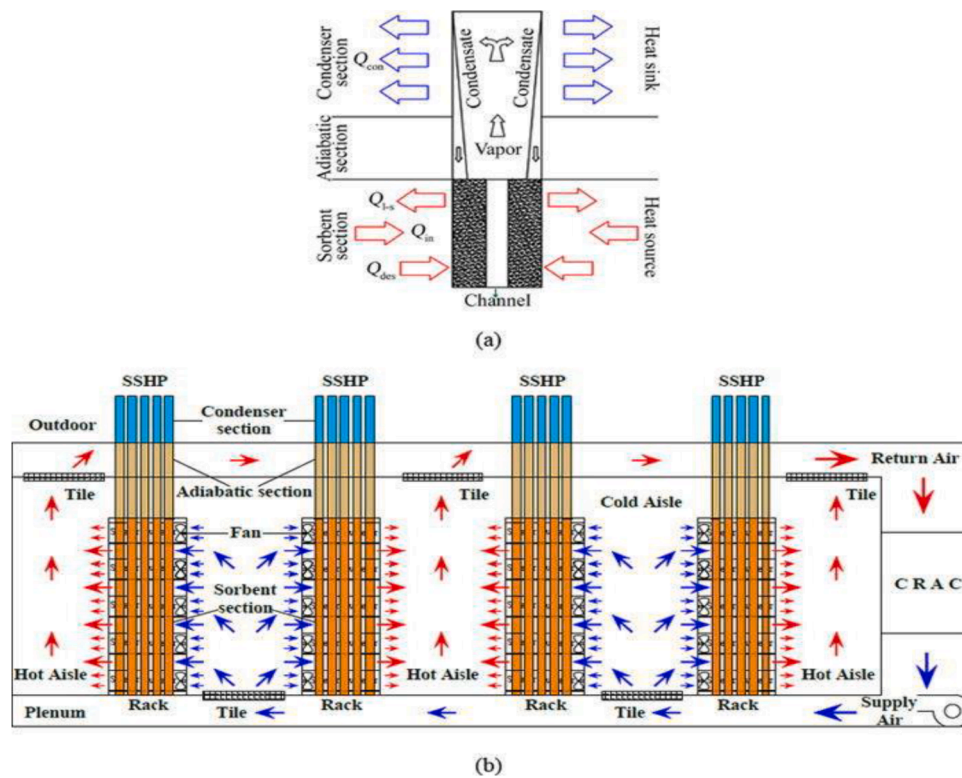

Fig. 13. Schematic diagram: (a) solid sorption HP unit and (b) thermal control system [136], reproduced with permission No. 5373,520,739,859.

system provided the healthiest supply and indoor air where the supply duct and indoor relative humidity (RH) were 68.4 and 51.1%, respectively. The total load of the air handling unit decreased as a result of the pre-cooling of the evaporator. According to the simulation results, 455 MWh was saved per year using eight-row HPHE.

Liu et al. [138] conducted a simulation on pre-cooled heat pipe (PCHP) for space cooling under high thermal density as illustrated in Fig. 14. Models of energy consumption and heat transfer for CHP and PCHP were built using MATLAB R2014a and the NIST REFPROP 9.1 was utilized to assess the thermodynamic properties of fluids and solids. The simulation of CHP without a cooling pad was conducted based on momentum, mass, and energy conservation. The ε-NTU method was applied in both the condenser and evaporator. The results indicated that increasing the thickness of the pad and flow rate, and decreasing the environment temperature and relative humidity (RH) enhanced the cooling capacity of PCHP. As well, at 20–40% RH, the energy efficiency

ratio (EER) increased and then decreased as the thickness of the cooling pad increased while at 70–90% RH, the EER decreased continuously. The cooling capacity of PCHP was found always to be higher than that of the CHP.

Zhu et al. [139] built an annual energy sing simulation module of a separated heat pipe (SHP) heat exchanger to evaluate the indoor air temperature and power consumption of AC systems for telecommunication base stations. The module was built using a simulation tool of DeST. The performance modeling of SHP using a gray-box model and the dynamic thermal process in building were conducted. Dynamic thermal features simulation was achieved to assess the room temperatures inside the building for varying the meteorological parameters, cooling/heating operation of the HVAC system, and internal heat gain. The comparison between SHP+AC and AC implied that the SHP+AC was an energy-efficient approach by utilizing natural cooling resources, particularly in the cold climate region. As well, optimizing the envelope
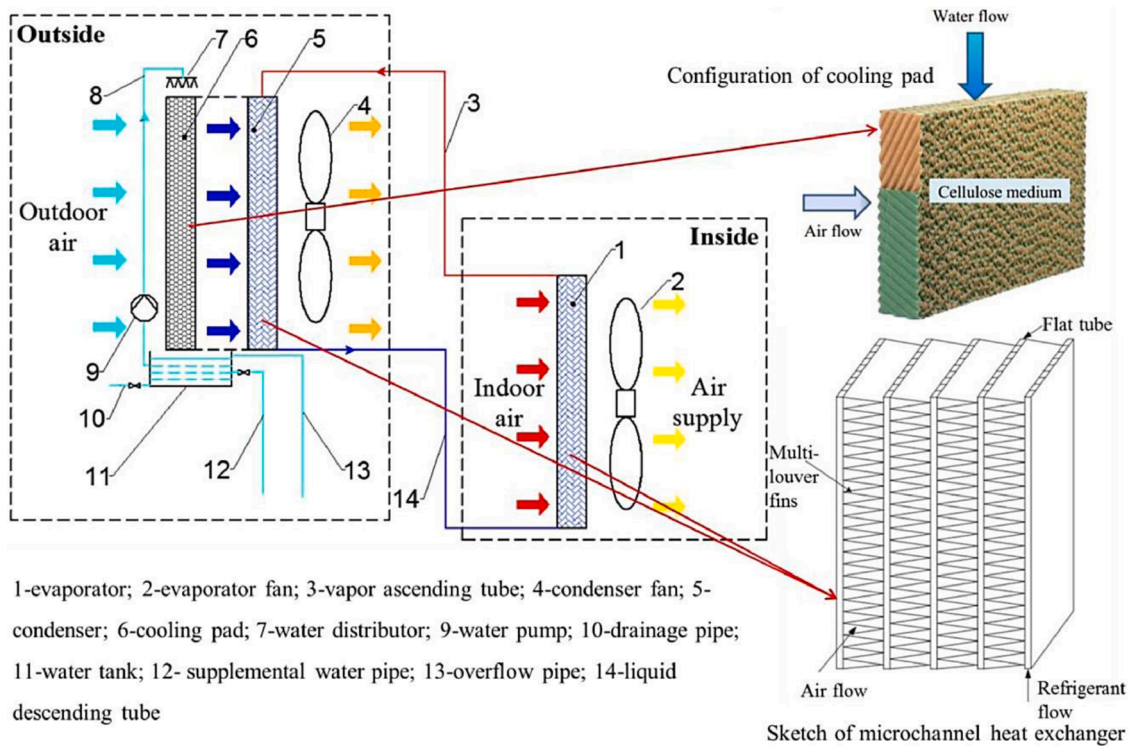
Fig. 14. Schematic diagram of PCHP [138], *reproduced with permission No. 5374,080,002,695.*

parameters and cooling scheme for different climate conditions and different power levels of communication apparatus was achieved with the SHP module. In addition, the effectiveness of the SHP heat exchanger was dependent on the difference between the outdoor and indoor air temperatures. SHP operation time had a high possibility of energy saving by employing evaporative cooling for outdoor units of dry climate regions.

Ling et al. [140] investigated the impacts of the environmental conditions and geometrical design on the thermal performance of a MCSHP for cooling purposes in telecommunication systems experimentally. A steady-state mathematical model was constructed to determine the mass flow rate of refrigerant, cooling capacity, overall h of
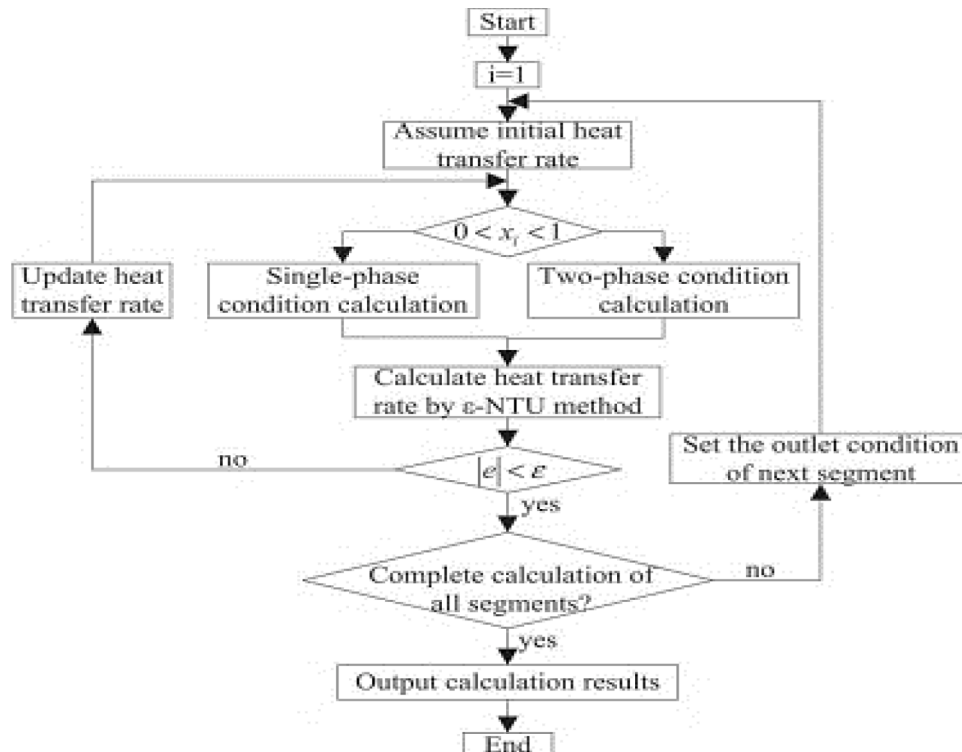

Fig. 15. Flow diagram for studying the performance of the MCSHP [140], reproduced with permission No. 5376060220463.

evaporator section, and the pressure drop of refrigerant and air using FVM. Each flat tube was split into 100 segments and the effectiveness-NTU method was employed to assess the characteristics of refrigerant and air. Fig. 15 shows the flow diagram for the different simulation steps of MCSHP. MATLAB R2007a was employed for solving the mathematical model and it was verified by comparing it with the experimental data. The simulation results revealed that the flat tube height had the highest effect on the pressure drop of the refrigerant which was reduced by 96.6% in a case of 3.0 mm compared with that of 1.4 mm height. The fin pitch had a maximum impact on the cooling capacity; the cooling capacity was improved by about 50.65% at 3.0 mm compared to 1.0 mm. Moreover, the cooling capacity was enhanced by 135% when the temperature difference between the outdoor and indoor was increased from 6 to 8 °C.

Du et al. [141] introduced a simulation model to estimate the performance of a greenhouse with a HP heating system. The simulation predicted the effect of the heating power required during the cold weather, heat losses from the greenhouse, and the maximum height. The output of soil and air temperatures was estimated by solving the model numerically according to the thermodynamics and heat transfer laws. The finite difference method (FDM) was used to study non-steady conduction through the soil. The results of the simulation were validated by experimentally obtaining data of air and soil temperature for winter conditions inside a greenhouse with an east-west (E-W) orientation located in the north of China. The air and soil temperatures were examined by changing different input parameters.

Yau [142] assembled an empirical transient systems based-TRNSYS model to evaluate the annual power consumption of a theater in Malaysia. The effect on the hour-by-hour energy consumption was simulated with experimental representations of two 8-row HPHEs installed in the HVAC system and was compared to the current HVAC system without the HPHEs. The simulation results of the TRNSYS HVAC model concluded that the employing of a double HPHE system had positively impacted the performance of the HVAC system in a hospital environment by enhancing the energy savings and moisture removal capability.

4.3. Nuclear reactors

HPs have been permanently investigated for advancing passive cooling systems in the area of nuclear energy reactors. Joeng et al. [32] conducted a two-step numerical analysis to assess the concept of a combination of a HP and control rod as a passive in-core cooling system (PINCs) for a sophisticated nuclear power plant. Firstly, the thermal performance of a single hybrid HP under extreme pressure and temperature conditions was evaluated by simulation using a commercial CFD code. Secondly, 1D thermal-hydraulic reactor under transient operation was accomplished using MATLAB to investigate the cooling effect of a hybrid HP as PINCs as presented in Fig. 16. The analysis of transient operation was performed by estimating the variation of coolant temperature inside the reactor pressure vessel with respect to the time after a reactor shutdown. 3D steady-state energy, momentum, and continuity equations were studied for solid, liquid, and vapor regions of a single hybrid HP using a commercial ANSYS-CFX code and Darcy's law was assigned for the wick porous media. The results indicated that about 18 kW of heat was transferred by a hybrid HP from inside to outside of the core and the R_{th} of the hybrid HP was 0.015 °C/W. In the transient analysis of the reactor, the boiling required time was delayed for 13 min when a hybrid heat pipe was used, and the core uncover time was postponed by 5.4 h which guarantees enough response time in case of accidents.

Kusuma et al. [143] investigated the thermal performance of a cooling system for a nuclear reactor with a spent fuel pool employing a vertical straight wickless HP. The effects of the initial pressure of HP, FR of the evaporator, evaporator heat load, and coolant flow rate were investigated. The simulation was conducted using a RELAP5/MOD 3.2 model for transient analysis to anticipate the behavior of the nuclear reactor during accidents and normal circumstances. The experimental and simulation results showed a similar pattern. Hence, the RELAP5/-MOD 3.2 proved its effectiveness for forecasting the process inside HP. The results demonstrated that the optimum thermal performance was at 0.016 and 0.014 °C/W approximately for the experimental and simulation results, respectively. The optimum results were achieved at high heat loads, a FR of 80%, and the lowest initial pressure.
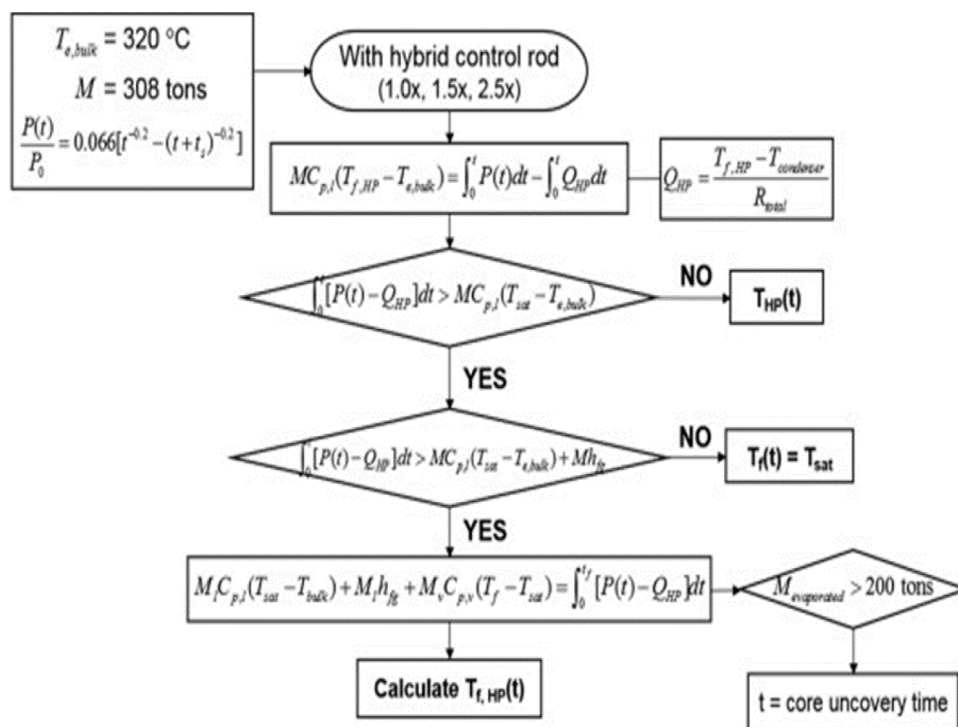

Fig. 16. Flow diagram of reactor analysis utilizing MATLAB [32], reproduced with permission No. 5373,521,214,193.

Kusuma et al. [144] conducted a simulation for a wickless HP as a cooling method in a nuclear reactor with a spent fuel pool. The impacts of FR and initial pressure on the thermal performance of HP under constant heat load, coolant mass flow rate, and temperature were studied. Thermal-hydraulics code RELAP5/MOD 3.2 was used to build and simulate the model. Each section of HP was split into 10 nodes to obtain better results for the simulation. The results demonstrated that the optimum performance was fulfilled at 74 cm Hg initial pressure and 60% FR. In addition, Xie et al. [145] conducted a 3D numerical model and experimental investigation to assess the heat transfer and turbulent flow of a HPHE applied to a residual heat removal system. A computational domain was a simplified model with a shell side and bundles of HP as presented in Fig. 17. The governing continuity, momentum, and energy equations were studied using a CFD model and the SIMPLE algorithm was used to solve the discrete dynamic equation for a given pressure field to obtain the velocity field. The heat transfer outside HP was investigated under different arrangements of pipe bundles, Reynolds number, and a number of rows. The results revealed that the maximum deviation between the experimental and simulation results was less than 10%. The maximum heat transfer power obtained from the simulation was 3.69 and 4.57 kW for different sizes of heat pipes of ϕ 16 mm x 2 mm and ϕ 19 mm x 2.5 mm, respectively. Avoiding the leakage of radioactive fluid and the high heat capacity of HP, the system introduced advantages for nuclear power applications.

Panda et al. [146] executed a numerical model of a high-temperature HP for heat removal passively in nuclear reactors. A 3D transient numerical model of HPs with square tubes using sodium as a working fluid was developed employing a general-purpose FEM code to assess the wall temperatures, vapor pressure, vapor core, and vapor velocity in a mesh wick of HP. The computational domain consisted of HP walls, wick, and vapor core was meshed using commercial software. The governing equations and boundary conditions employing staggered mesh were discretized using the implicit FVM. The coupling of pressure and velocity was conducted by the SIMPLE algorithm. A successful test of HP was conducted with an input heat transfer of 40 kW/m^2 and temperature flattening happened within 14 operating hours. The experimental and simulated values of surface temperatures were close to each other and the maximum variation was 1.25%.

Kuang et al. [147] modeled and simulated a large-scale separated HP for fuel pool cooling with low heat flux. A numerical model was initially conducted and then justified according to prior experimental results. The effects of connection pipe length and the heat source temperature were investigated. Water, R134a, and ammonia were used as working fluids. The evaporator of a straight fin tube was heated via hot water, and the condenser of a circle fin was cooled via air convection. Significant pressure losses in water HPs occurred due to the long-distance heat transport and hence the heat transfer performance was reduced significantly. R134a and ammonia heat pipes were more appropriate for long transport distance situations. The results demonstrated that the reduction in heat transfer rate was almost zero, 4.1%, and 55.9% for ammonia, R134a, and water, respectively. The vapor quality at the evaporator exit was less than one for all simulations. Vapor quality at the exit of the condenser section was zero, and the descending tube was somewhat liquid-filled. Moreover, the heat transfer increased with increasing heat source temperature, while for water, the heat transfer increased inconsiderably, and it was almost constant from 77 to 85 °C due to the water's low quality of vapor at evaporator exit and more liquid delivered to the condenser led to a deterioration in the condensation heat transfer. For R134a and ammonia, annular flow and slug flow couldn't be maintained in the evaporator section and the nucleate
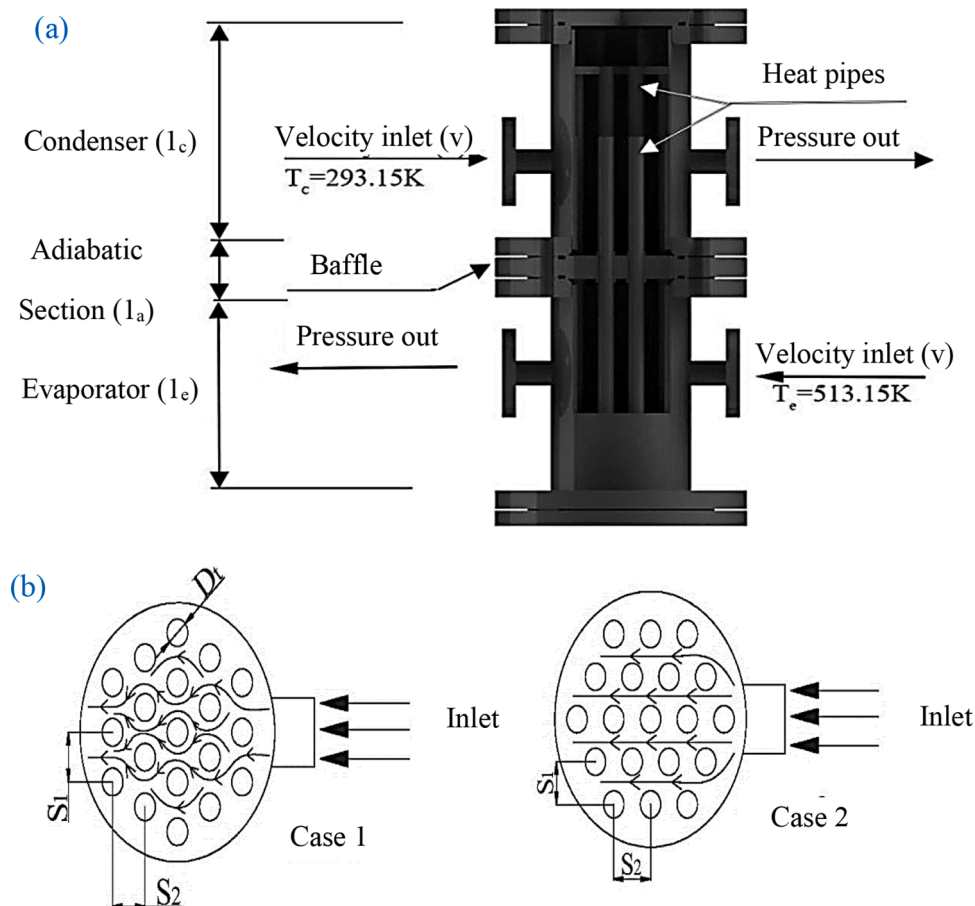

Fig. 17. (a) View of the HPHE and (b) two bundle arrangements [145], reproduced with permission No. 5373,521,324,965.

boiling was the essential mechanism of heat transfer due to small surface tension and low wall heat flux.

4.4. Solar energy systems

The utilization of solar energy includes a number of critical applications such as photovoltaic (PV) modules [148–151], building-integrated photovoltaic/thermal (BIPVT) [152, 153], zero energy building [154], water desalination [155–158], etc. The HPs are employed in different applications of solar energy such as water heating systems [159], evacuated tube solar collectors [160], solar HP thermoelectric generators [161], and solar-assisted heat pumps [162].

He et al. [161] developed an analytical and simulation model for the condition of constant solar irradiation to analyze the performance of a solar heat pipe thermoelectric generator (SHP-TEG). Solar irradiation, cooling water temperature, a number of thermoelements, and cross-section area and length of thermoelements were studied. SHP-TEG operated under the electrical power priority model and electrical power and hot water model. The simulation for different operating and design parameters was conducted. The maximum efficiency was 3.346% occurred at a thermoelement length of almost 2.5 mm. Furthermore, Zhang et al. [163] investigated the performance of HP in a photovoltaic/thermal (PV/T) system with various circulation tank capacities. The numerical model was developed using TRNSYS to optimize the system orientation and tilt angle and system tank volume and to calculate the electric power. Fig. 18 indicates that the temperature of PV is higher for lower volume at the same time interval. The generation efficiency was lower for low volume tanks and the optimum value of 80 L for heat collection and power generation accomplished the maximum overall efficiency of 67.5%. The average annual power generation efficiency and the average annual collection efficiency were 15.69 and 34.37%, respectively.

Dai et al. [164] developed and simulated a hybrid photovoltaic solar-assisted loop heat pipe/heat pump (PV-SAHLP/heat pump) for a water heating system. The system was integrated with a PV/T

evaporator, compressor, water tank with a flooded condenser, and a thermostatic expansion valve. The results demonstrated that the overall efficiency was 33.7%. As well, the optimum operating time for the LHP/heat pump mode was in the spring season while the HP mode was the best suitable for winter. The monthly power consumption of LHP/heat pump mode was about 13.9% lower than that of heat pump mode while the monthly mean overall efficiency for the heat pump mode was higher.

Li et al. [165] investigated the effect of evaporator temperature and tilt angle (θ) on the thermal performance of a MCHP employing the ANSYS fluent program. The variation of the wall temperature of HP and the thermal conductivity were evaluated. A 3D multiphase model with a mixture model was employed. Several phases could be modeled using the mixture model by solving the continuity, momentum, energy, relative velocities algebraic, and secondary phases volume fraction equations. The results demonstrated that at an evaporator temperature of 50 °C, the largest temperature difference was detected for a θ of 40 °. The temperature gradient was lower at a θ of 50°, due to better heat transfer performance. In addition, the MCHP's effective thermal conductivity and temperature distribution greatly rely on tilt angles along with the temperature of the evaporator. The temperature fluctuations in the microchannel increased as the θ increased. At lower values of θ, higher temperature of the evaporator, and higher temperature difference, the optimal θ was in the range of 50– 70° for different evaporator temperatures. Gang et al. [166] designed and constructed a heat-pipe photovoltaic/thermal system (HP-PV/T) followed by the development of a dynamic model to assess the system performance as shown in Fig. 19. The numerical results revealed that the system's electrical and thermal efficiencies were 9.4 and 41.9%, respectively. Whereas, the average electrical and heat gains were 62.3 and 276.9 W/m², respectively.

Albanese et al. [167] carried out a simulation and an experiment to evaluate the performance of a HP-assisted passive solar space heating system to transfer heat from an absorber to an indoor storage tank. The system performance of indirect gain, direct gain, and integrated HP passive solar systems were simulated for different climates by
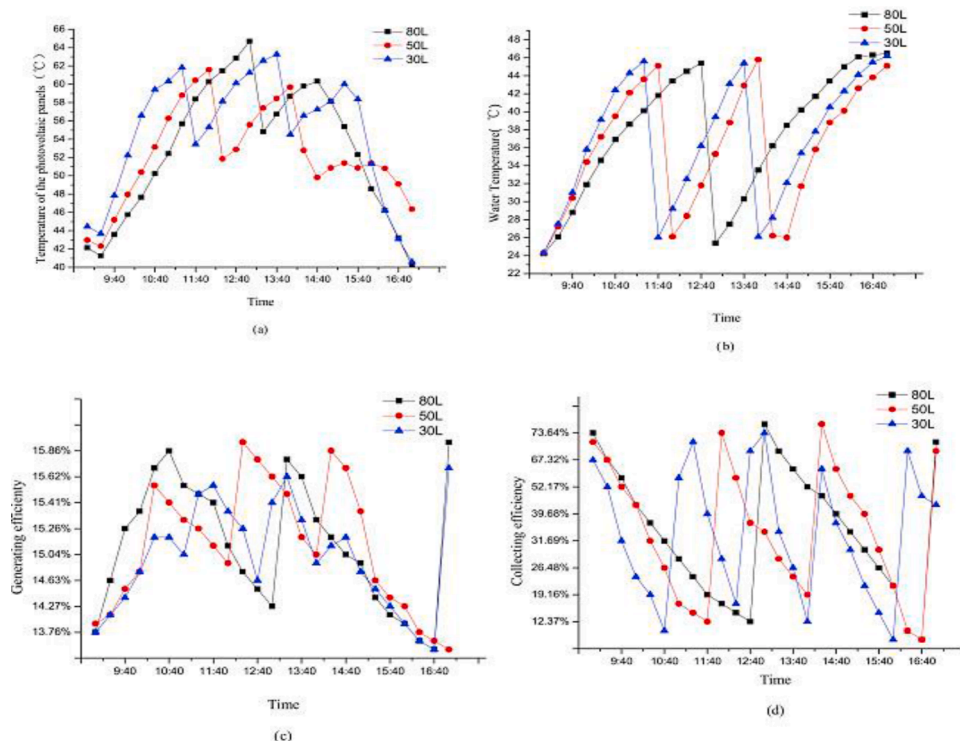

Fig. 18. (a) Temperature of PV panel, (b) change of water temperature, (c) electrical efficiency, and (d) collection efficiency for different tank volumes [163], *reproduced with permission No. 5373,570,874,465.*

Fig. 19. System illustration (a) HP-PV/T solar collector and (b) cross section of solar collector [166], *reproduced with permission No. 5373,571,341,014.*

constructing simplified thermal resistance using MATLAB. In addition, a parametric study was conducted to investigate the influences of design features on the system performance. The *h* was calculated by a series of

iterations by simultaneously the governing equation. Regarding absorbed solar radiation, an anisotropic model that contains various components of diffuse radiation: horizon brightening, circumsolar, and

Fig. 20. Thermal networks for passive solar computer simulations [167], reproduced with permission No. 5373,571,463,337.

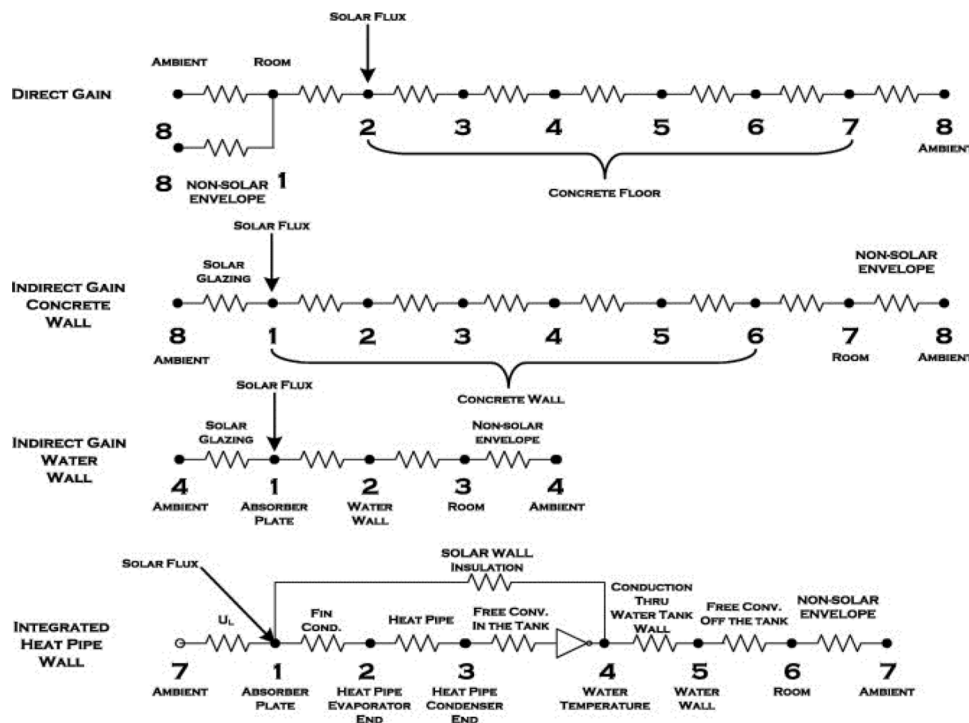uniform was employed. The heat transfer modes for each network conductance value are presented in Fig. 20. The thermal diode of HPs provided efficient heat transfer into storage and less losses in the opposite direction, thus, the simulated system performance was considerably higher than that of the direct and indirect gain passive solar systems for all climates examined conditions. Adding nighttime insulation to the direct and indirect gain systems reduced the losses while it achieved high R-values because automatic or manual control was required. The highest efficiency was about 0.85 achieved at a 120% charging fill level.

Alizadeh et al. [168] simulated numerically the PV cooling by employing a single turn PHP another with a copper fin. The simulation was conducted considering an ambient temperature of 291 K, 1000 W/m^2 heat flux, and the condenser temperature of PHP was equal to the ambient temperature. The results indicated that the PHP accomplished a greater temperature reduction than the copper fin. In addition, cooling with PHP required less time to reach a constant working temperature. The temperature contours across the PV panel as presented in Fig. 21 and it is observed that the highest temperature was recorded at 309.4 K maintained at the panel corners, and the lowest temperature was about 305.0 K. PHP system achieved a maximum reduction of temperature difference of almost 16.1 K, while the copper fin had only reduced the panel's temperature by a maximum of 4.9 K. In addition, the PHP system enhanced the electrical power generation by 18% while the copper fin system increased the electrical power generation by only 6%.

4.5. Electric vehicles

Electric vehicles (EVs) that can decrease the emissions of greenhouse gasses (GHG) store considerable energy inside mainly lithium-ion (Li-ion) cells [169–171]. Currently, the existing battery's cells should be utilized to the maximum potential due to their high costs and restricted-energy density. Maintaining the optimal operating operation and maximizing the lifetime introduces the opportunity for the world-wide spread of EVs [172–174]. The cell temperature is the most influential parameter that has a critical impact on the execution chemistries degradation of Lithium-ion [38, 175, 176]. As well, the temperature gradient of the battery rather than the maximum temperature contributes to cell aging. So, the batteries thermal management system (BTMS) in EVs to regulate the temperature and extend the battery lifetime by prolonging the Li-ion cells' lifetime is essential by using different cooling methods such as phase change material, liquid cooling, heat pipes, etc., [177].

Lei et al. [178] optimized and designed sintered heat pipes using water sprays at the condenser section to manage the temperature of batteries for EVs. The results demonstrated that the maximum temperature and the maximum temperature difference of battery due to using thermal management systems (TMSs) were reduced by 29.2 and 8.0 °C, respectively. Additionally, the performance of the cooling system for TMS-based copper tubes and HPs was numerically investigated by Wan [179]. The main findings indicated that HP lowered the battery maximum temperature and the temperature difference compared with copper rods by 41.6– 60% and 89.8– 90.6%, respectively.

Deng et al. [180] analyzed the feasibility of waste heat recovery (WHR) from coalfield fire using an integration between HP and thermoelectric generator (TEG). As well, a numerical assessment-based thermal equivalent model was proposed. The results revealed that the waste heat flow and the average utilization rate were 495 W/m^2 and 58%, respectively. In addition, the cooling source, heat source, and thermal resistance of HP were 0.00195511, 0.0021732, and 0.0048988 W/ °C, respectively. Finally, the estimated WHR from the overall fire field of 105 MW/a was employed for district heating, electric power generation, and provision of the required water for fire extinguishing. Additionally, the performance of HP combined with a thermoelectric cooler (TEC) for BTMS in electric vehicles was investigated numerically and experimentally by Zhang et al. [181]. 3D Fluent software, based on Solidworks of Dassault Systems was employed. The results revealed that the proposed cooling system reduced the battery surface temperature significantly at different discharge rates. Moreover, the proposed system maintained the battery's temperature within 318 K at a discharging rate of 3C.

Hong et al. [182] utilized ultra-thin loop-heat pipes (ULHPs) with 1.5 mm thickness of flat evaporators for flaked LiBs considering the impacts of entrance length, groove shape, thermal resistance, system start-up, groove shape, heat leakage, and condenser position on the operation temperature. The findings demonstrated that the ULHPs maintained the appropriate batteries thermal management with a temperature of less than 50 °C for the optimum structure that reduced the heat leakage and decreased the R_{th} and temperature.

Zhao et al. [183] designed and examined a HP combined with phase change material (PCM/HP) for BTM of cylindrical power batteries in EVs. The results revealed that for the same conditions, the PCM/HP ensured the maximum temperature (T_{max}) under 50 °C for an extended time duration than only phase change material (PCM) or air-cooling systems. Furthermore, the TMSs-based PCM/HP managed the battery temperature difference under 5 °C. In addition, Jiang and Qu [184] investigated the battery temperature for different charge/discharge cycles using PCM/HP. The lumped thermal model was employed
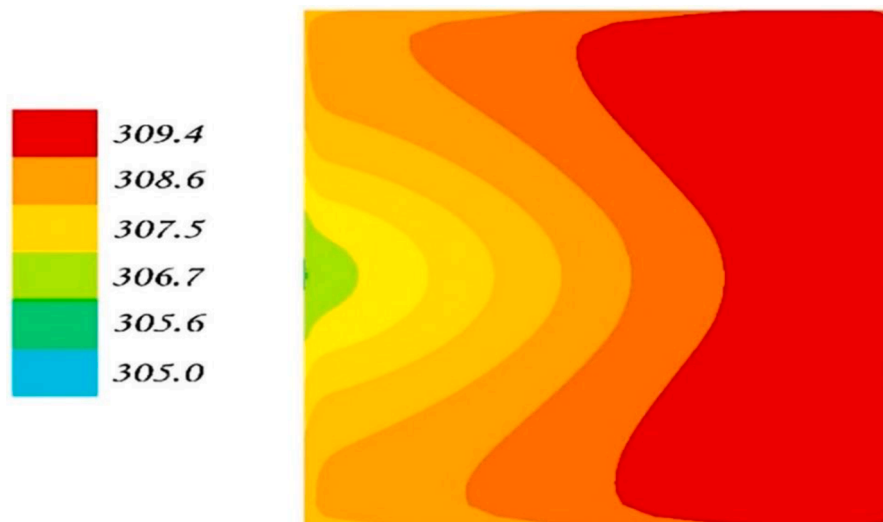

309.4
308.6
307.5
306.7
305.6
305.0

Fig. 21. Contour of surface Temperature of PV panel at a solar intensity of 1000 W/m^2 [168], reproduced with permission No. 5373,580,056,004.

considering the melting of PCM, battery heat generation, and transient thermal response of HP. The results revealed that using HPs recovered the latent heat from PCMs with a convenient melting and maintained the low temperature of the battery for an extended long period. In order to guarantee the appropriate energy density for long-term cycling, low energy consumption, and safe temperature, the PCM melting point should be greater than the ambient temperature by 3 °C, and the h of the condenser was between 30 and 60 W/m^{2}K using an optimum phase change ratio (PCR) and thickness ratio of 0.55 and 0.17, respectively. The temperature and PCR of HP/PCM under various ambient temperatures are represented in Fig. 22.
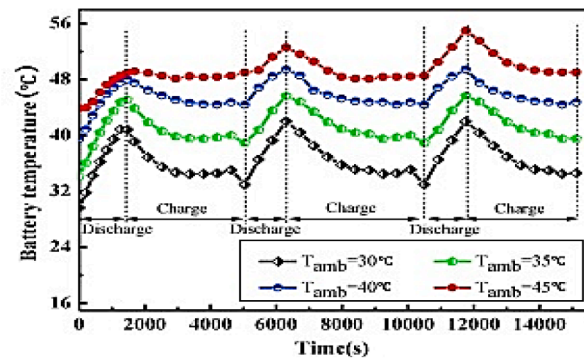
Behi et al. [185] assessed the performance of a lithium titanate cell under different cooling strategies: flat HP-assisted, forced fluid cooling, and natural air cooling for EVs experimentally. The results revealed that only one HP at a critical region was demanded to maximize the heat dissipation. Furthermore, the proposed cooling methods were investigated via a 3D computational fluid dynamic (CFD) COMSOL Multiphysics model to assess the cooling capacity of two methods: liquid cooling and liquid cooling method integrated with heat pipe (LCHP). At a discharging rate of 8C, the single HP delivered almost 29% of the required cooling load. Moreover, both liquid cooling and LCHPs significantly decreased the temperature compared to natural air cooling by 29.9 and 32.6%, respectively. Fig. 23 introduces the temperature contour of the module for different cooling systems.

TMS-based HPs for cylindrical cells battery application was studied numerically by Wang et al. [186]. For the BTMS, a CFD model was introduced using ANSYS Fluent to determine the influence of different parameters such as battery spacing, thickness and height of the conduction element, and the circumference angle between the conduction element and battery on the thermal performance. It was noticed that the conduction element height influenced the maximum temperature and temperature difference of the battery. Additionally, the angle between the conduction element and battery was the second sensitive factor. On the other hand, the battery spacing and the conduction element thickness had a mi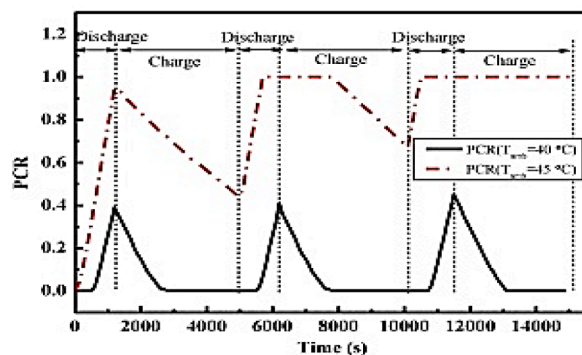nimal influence. The efficient performance was accomplished when the battery spacing, and thickness and height of the conduction element, and circumference angle were 19, 4, 60 mm, and 120°, respectively. The corresponding battery temperature difference and the maximum temperature were 1.08 and 27.62 °C, respectively.

Dan et al. [187] developed a TMS for operating in aggressive circumstances using a micro/miniature heat pipe array (MHPA). Using the AMESim environment, a numerical thermal model of MHPA was developed. The results revealed that the MHPA ensured the battery temperature under 40 °C for a 1C discharge rate employing natural convection. Additionally, a 3C discharge rate with a 3 m/s of air velocity fulfilled the heat dissipation requirement. Furthermore, using MHPA for battery pack enhanced remarkably the uniformity of battery temperature and controlled effectively the temperature. Using Al$_2$O$_3$ nanofluid filling the HPs for TMS of LiBs in electric vehicles was investigated numerically by Nasir et al. [188]. The results indicated that utilizing a 1.5% volume concentration of Al$_2$O$_3$ nanofluid lowered the overall thermal resistance compared to water-filled heat pipes by roughly 15%, and resulted in a reducing the surface temperature of the battery by 4.4 °C with 7.28%.

Bernagozzi et al. [189] conducted a 1D lumped parameter network (LPN) simulation of a LHP for heating/cooling thermal management systems in a fully EV. The LPN model was used to avoid the complexity of integrating mass, momentum, and energy balance equations and to significantly reduce the computational time. The proposed approach for the condenser analysis was introduced accurately to guarantee mass conservation with various integration time steps and boundary conditions. The feasibility of implementing LHPs in fully electric vehicles, and two different condenser configurations were examined. Where in the first design, four equal condensers along the whole length of the underbody were subjected to three values of h while in the second design, three different condensers were employed in a zone and subjected to a single h. Both designs proved the ability to remove the required heat loads.

(a) Temperature variation in the module under different ambient temperatures based battery cooling system

(b) PCR variation in the module under different ambient temperatures-based battery cooling system

Fig. 22. Temperature and PCR for HP/PCM under different ambient temperatures [184], *reproduced with permission No. 5373,580,436,868.*
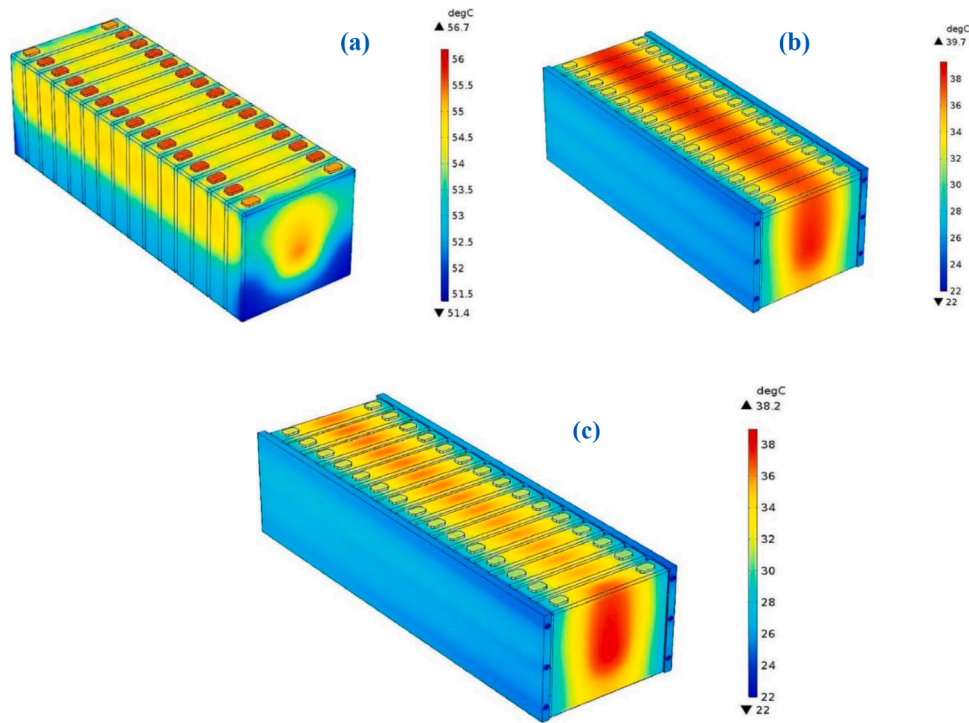
Fig. 23. Module temperature contour for: (a) natural air cooling, (b) liquid side cooling, and (c) liquid side cooling and HP [185], open access.

4.6. Wast heat recovery systems

HPs heat exchanger proposed a waste heat recovery (WHR) system for hospitals and laboratories [190]. Burlacu et al. [191] introduced an energy-efficient HP heat exchanger used for WHR in buildings for air heating using a CFD. The numerical results demonstrated that the HP heat exchanger operated effectively with a high-volume flow rate of a secondary agent or with a low-temperature of the primary agent. As well, Yang et al. [192] studied numerically and experimentally the feasibility of WHR-based HPHE for heating purposes of automobiles employing the exhaust gas. HP was made from steel with a working fluid of water and occupied about 35% of evaporator volume. Keeping the cold air inlet temperatures at 8 °C, the heat transfer rate for various exhaust gas inlet temperatures i.e., 100, 200, and 300 °C was evaluated. The results indicated that rising the inlet temperature of exhaust gas improved the rate of heat transfer.

Fierro et al. [193] investigated numerically and conducted a techno-economic assessment of WHR system-based capture of radiative heat transfer from a rotary kiln. It was observed that a potential heat recovery accomplished a temperature of 240 °C and potential of heat recovery up to 4980 kW with exergy and thermal efficiencies of 48.62 and 17.35%, respectively. Finally, Lin et al. [194] studied numerically the performance of HPs for WHR to intensify the dehumidification process using a CFD package of FLOTHERM. The drying cycle in conjunction with Excel calculation was employed to simulate a two-phase process. The results revealed that increasing the air flow rate and inlet temperature introduced a superior thermal performance of the drying cycle system. The study predicted that the HP further enhanced the system performance greater than the auxiliary condenser.

4.7. Cryogenics

Most thermal systems-based HPs are involved with heat sources at high-temperature while research areas for extremely low-temperature such as cryogenics has a scientist's attention [77]. Similar to the conventional PHPs, the inclined angle of HP influence the performance of cryogenic PHPs [195]. Qu et al. [196] introduced a model of cryogenic

LHP considering the variation of mass flow rate and the subcooled effect. The heat leak was estimated on the basis of 1D temperature distributions in the evaporator with varying parasitic heat load, filling pressure, and auxiliary heat load. The results revealed that voiding the fraction of the primary compensation chamber was the determinant factor for minimizing the working heat load. However, voiding the fraction at a low filling pressure less than 1.4 MPa and the maximum capillary pressure at a high filling pressure greater than 1.4 MPa maximized the working heat load.

Singh and Atrey [197] numerically simulated the working of a nitrogen-based PHP. In the numerical model, a slug-merge subroutine was employed to evaluate the collapse of vapor plugs. The influences of different operational and geometric parameters on heat transfer mechanism were presented. The results revealed the presence of an optimum inner tube diameter of 1 mm for a 20 turns and a fill ratio (FR) of 0.3 maintained the peak performance. In addition, Sagar et al. [198] introduced a two-dimensional numerical physical model of a three-turn cryogenic PHP of liquid nitrogen for cooling superconductors. The VOF model was employed to simulate a two-phase flow in a cryogenic PHP for FR ranging by 25–70%, the evaporator temperature within 85–115 K, and 76 K condenser temperature. Autocorrelation function (ACF) and power spectrum density (PSD) tools were used to study the wall temperature-time series. The results revealed that increasing the heat input from 85 to 115 K by 35% increased the working fluid temperature gradient by 250, 182, 85, and 186% for a FR of 25, 42, 55, and 70%, respectively. The local temperature contours for different FRs for evaporator temperature of 95 K and condenser temperature of 76 K with an anti-clockwise direction of the flow circulation are presented in Fig. 24.

4.8. Other applications

Sharifi et al. [199] accomplished simulation of an integrated HP located in a vertical cylindrical enclosure filled with PCM and assisted energy storage system based-latent heat thermal in which the HP is concentric. PCM was placed around the middle part of HP, while the bottom and top parts are exposed to heat for different methods of
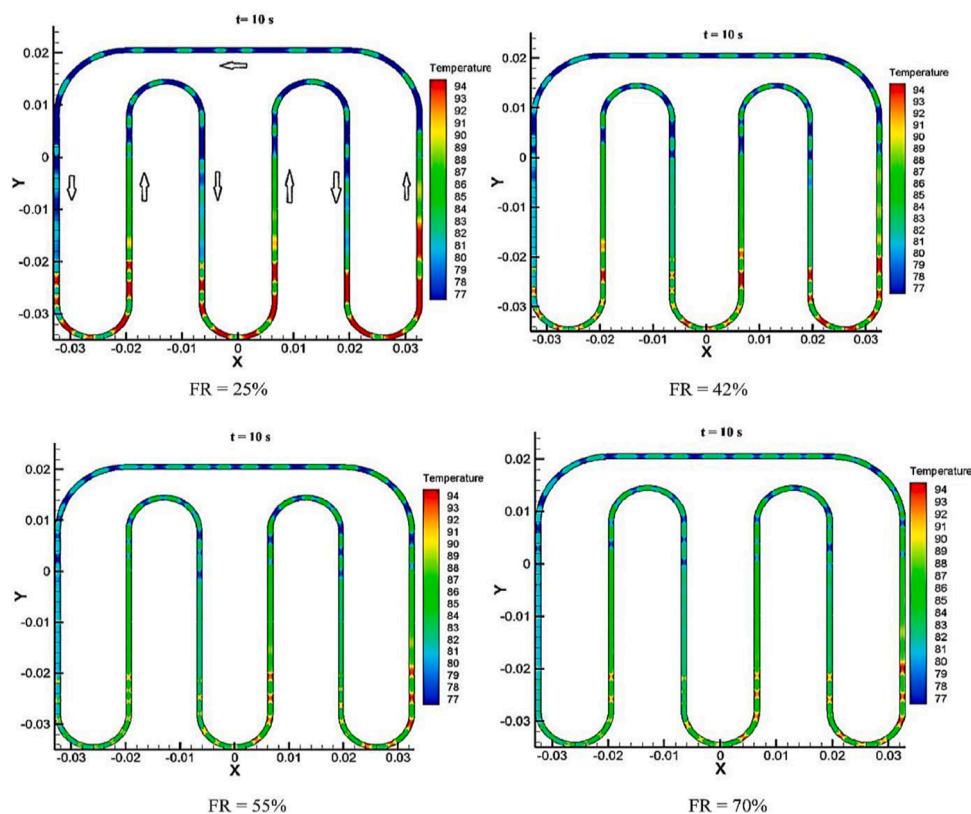
Fig. 24. Local temperature contours for different filling ratios (FRs) [198], Reproduced with permission No. 5374,080,074,618.

operation e.g., charging only, charging/discharging simultaneously, and discharging only. A parametric study was performed to investigate the impact of the input/output heat transfer rates and PCM enclosure height. It was concluded that for the same amount of PCM, a larger height-to-diameter ratio showed a lower average bottom wall temperature of HP and hence enhanced the melting during simultaneous charging and discharging. This was due to a larger heat transfer area and a short conduction distance in PCM. Moreover, increasing the input and/or output heat transfer rate had an impact on the heat pipe top and bottom sections' temperatures, while only a minor effect on the middle section's temperature. Ramos et al. [200] studied the thermal performance of cross-flow HPHE experimentally as well as numerically using a CFD ANSYS Fluent model. The examined HPHE consisted of an evaporator, condenser, and six water-charged wickless HPs. The results revealed that the heat transfer rate was directly affected by the mass flow rate and temperature and the achieved heat transfer rate was up to 900 Watt/pipe.

Currently, hydrogen is used primarily in the chemical industry as well as it will be a significant fuel in the near future. There are a number of technologies for hydrogen production from both fossil and renewable biomass resources [201]. Today, in commercial use, the fuel processing of methane is the common method of hydrogen production. Recently, there is an international attention on the development of new technologies of hydrogen as a potential choice for the current scare and to increase the security of energy and the economic. Chen and Wang [202] studied the intensification of methane autothermal reforming (ATR) for hydrogen production using a novel HP and the folded reactors numerically employing CFD and CHEMKIN software. The performance indicators of the reactor such as hydrogen yield, rate of methane conversion, and the temperature difference between the reactor outlet and inlet, were computed and compared to those of the conventional tubular reactors. The results indicated that under optimum operating parameters, the heat pipe reactor and the folded reactor increased the rate of methane conversion compared to the tubular reactor from 34 to

45% and 50% while it enhanced the hydrogen productivity from 22.2 to 28.6%, and 31.4%, respectively. As well, putting the HP closed to the reactor front improved the catalyst activity and caused a rate enhancement of methane conversion.

Wang et al. [203] developed a MAGNET facility using Multiphysics Object-Oriented Simulation Environment (MOOSE) software and System Analysis Module (SAM) codes to duplicate the microreactor design based on HP cooling technology for hydrogen production. The results showed that each progressive set of HPs about its center increased the heat load inside the monolith. Additionally, the heat pipe failure and the peak temperature were directly proportional. Shatat and Mahkamov [204] evaluated the performance of a multi-stage water desalination still system integrated with a HP solar collector with an evacuated tube experimentally and numerically. The water desalination system with a multi-stage solar still was proposed to recuperate the available latent heat from condensation and evaporation processes through four stages. The results demonstrated that the desalination proposed system produced about 9 kg of freshwater/day with an efficiency of solar collector of 68%. and the overall efficiency was 33%.

A numerical model of HPHE that included 18 rows of HPs with 9 pipes for each row was presented using a computational fluid dynamics (CFD) code by Jouhara et al. [205]. The numerical results of pressures and temperatures for evaporator and condenser are reported in Fig. 25. It is noticed that the temperature reduces in the evaporator from 210 °C to approximately 145 °C. As well, the maximum pressures for the evaporator and condenser were observed at the inlet. Additionally, distributed and lumped parameters model of the ceramic industry was constructed using the LMS Imagine. The results revealed that the application of HPHE to cool the stack of ceramic kiln facilitated the recuperate of greater than 863 MWh of thermal energy employed for heating air stream for pre-kiln dryer.

Jen et al. [206] conducted an experimental and numerical study to investigate the feasibility of utilizing HP cooling for drilling applications. The influences of different geometric parameters of drill
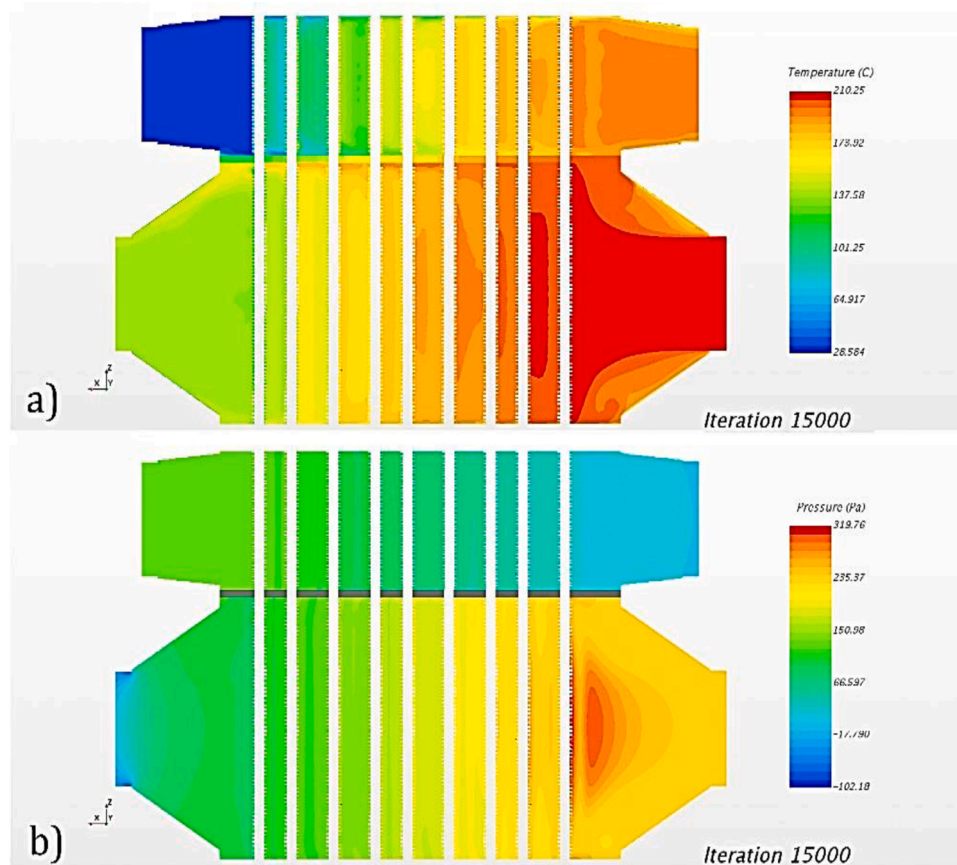
Fig. 25. Numerical results of: (a) temperature distribution and (b) pressure variation on evaporator and condenser [205], open access.

configuration of HP such as depth of HP within the drill, the diameter of HP, heat flux input, and zone length of heat input. The numerical model was carried out by a FEM and a commercial code of Pro-Mechanica was utilized to assess the temperature distribution in the steel cylinder. The results can be used to identify the geometric parameters for the optimal system design.

5. Summary and discussion

The utilization of HPs for different applications in diverse engineering aspects is effective and beneficial, and they are applicable for a broad range of operating temperatures. Table 1 summarizes the simulation modeling methods for different types of HPs. It is noticed that there is considerable progress in the modeling of HP systems in a wide range of engineering applications. It can be seen that most studies are centered mainly on LHPs and pulsating/oscillating HPs. Heat flux/input is the most frequent tested parameter [93, 106, 112, 113, 125]. Other common parameters are the working fluid and/or FR such as in [113, 120, 121], and the wick structure and/or its porosity such as in [78, 104, 109]. Despite that not all software used is mentioned, it is noticed that the ANSYS FLUENT is common relatively. Most of the simulations have been done on HVAC, nuclear, and solar systems either PV or thermal heating systems. It is clear that due to the difference in performance nature of different types of HPs so they are found in various applications. It is observed that there has been massive progress in the optimization of CHP.

The simulation modeling for different types of HPs was conducted in diverse applications including thermal management for space systems and satellites, vapor plugs and liquid slugs in nuclear reactors, telecommunication industry, solar thermal collectors, cooling of electronics, thermal energy storage, light-emitting diode, HVAC, greenhouse, and thermoelectric power generation. Moreover, there is a variety in the employed software compared such as RELAP5/MOD3.2 [143] for nuclear applications, MATLAB [138] and TRNSYS [142] for HVAC systems, and FORTRAN [161] and ANSYS fluent [165] for solar energy applications.

6. Challenges and recommendations for future research

Recently, simulating the heat pipe systems that have great attention, however there is still an extensive gap in the available literature that is required to be covered to study accurately the fluid flow and heat transfer characteristics of HPs as well as the system cost. There are a number of critical challenges that must be investigated in future work to well investigate the heat pipe performance for different applications. The conducted progress on the numerical simulation of HPs is extremely acceptable while maximizing the performance of HP by minimizing the system's cost for various applications will make the technology more pronounced for commercial applications. So, the trade-off of performance-cost should be investigated to maintain a balanced midpoint to make the technology more feasible. Limited investigations are concerned with minimizing the capital initial and operating and maintenance costs by maximizing the system thermal performance.

Based on the numerical results of the achieved investigations, optimizing the thermophysical properties of working fluids e.g., thermal conductivity, specific heat, viscosity, latent heat of vaporization, triple and critical points, and surface tension on the thermal and fluid flow behaviors should be investigated. In addition, conducting a sensitivity analysis for studying HPs to a particular application is required to identify the most influenced geometry and operating parameters on the HP performance. Studying the numerical modeling of various HP systems, such as separated heat pipe (SHP), loop heat pipe (LHP),

Table 1

Summary of numerical simulation investigations of different types of heat pipes.

Ref.	Application	Type of HP	System description	Simulation software	Input parameters (variable parameters)	Investigated Parameters	Model dimensions
[32]	Nuclear reactors	Hybrid heat pipe	Hybrid HP with control rod as a passive cooling system in nuclear reactors	ANSYS-CFX	Temperature change of the coolant	Thermal performance or cooling effect	1D
[136]	HVAC	Solid sorption heat pipe	Control system integrated by a solid sorption heat pipe with air convection for cooling of data center	SolidWorks flow simulation	Different types of composite sorbents under cold source temperature	Fluid flow and temperature variation for room of data center and rack level	3D
[78]	Rack level cooling	CHP	Thermal control of internet data centers in rack level	Ansys FLUENT with SIMPLE algorithm	Thermal Conductivity of HP, wick porosity, transmitting heat power, radius and length of HP	Outer surface temperature distribution, pressure distribution, and thermal resistance	2D
[91]	Thermal management applications	(PHP	Two-phase flow boiling onset, formation of slug and plugs, and flow patterns	Eulerian approach	FR of the working fluid, heat input flux, and orientation of HP	Thermal performance and total liquid momentum	1D
[92]	Bubble generation	Multi-branch PHP	Bubble and film occupied the tube cross-section	CASCO software	Tube heat conduction and bubble generation	Start-up, functioning, and dry-out of PHP	2D
[93]	Vapor plugs and Liquid slugs	PHP	Multi-Phase flow	ANSYS-CFX	Heat input and FR for evaporator of methanol and air	R_{th} and temperature or temperature distribution	1D
[94]	Oscillating motion and temperature change as a result of evaporation and condensation maintained in MOHP	MOHP	Heat transport capability of MOHPs	VOF, mixture model in FLUENT and continuum surface force (CSF)	Length and inner diameters at various heating powers	Thermal performance including temperature distribution and R_{th}	2D
[95]	Bubble generation	OHP	Oscillating motions for vapor plugs and liquid slugs with large amplitude	FORTRAN codes	Tube-size bubble generation	Liquid slugs flow behaviors, vapor plugs, and the characteristics of heat transfer	1D
[104]	Bimodal porous medium	LHP	Explanation of porous medium of throats and cubic network of pores	Mesoscale approach, FVM, and mixed pore network model	Wick/capillary structures	Evaporator thermal performance	3D
[105]	Leakage of heat form capillary wick and shells	LHP	Surface thermal insulation between shells of evaporator and compensator	ANSYS fluent and VOF multiphase flow model	Alumina-copper coating, operation stability, temperature changes, and water volume fraction distributions	Temperature and water volume fraction distributions	3D
[106]	Electronic devices	LHP with flat evaporator	Two-phase interface distribution and dynamics through the porous wick	Advanced phase-change Lattice Boltzmann approach	Heat flux and surface wettability or contact angle	Dynamics of the interface of liquid-vapor, liquid volume fraction, temperature distribution at wick-groove interfaces and wick-fin, and overall performance	2D
[107]	Power or sink cycles including startup	LHP with stainless steel/ammonia	Time-dependent conservation equations	Software tool EcosimPro, homogenous equilibrium model, DASSL method	Surrounding environment (ambient and vacuum)	Overall dynamic behavior of an LHP	1D
[108]	TacSat-4 satellite LHP	LHP	Navier–Stokes equations for vapor flow and liquid zones and Darcy's law for filtration	SST turbulence model, SIMPLEC algorithm	Evaporation on interfaces between vapor regions and porous and vapor grooves	Heat and mass transfer, variation of pressure, and Vapor velocity distributions	3D
[109]	Liquid thin-film theory and interface of liquid–vapor through the capillary wick	LHP with flat evaporator	Analysis of evaporator comprising a capillary structure	Kinetic theory of gasses and liquid thin-film theory	Length of condenser, the porosity of capillary structure, and vapor temperature drop	Overall heat transfer performance	1D
[110]	Thermal management devices	LHP with flat and cylindrical evaporators	Steady-state analysis of capillary structure comprising fine pores	Theories of liquid thin-film and kinetic of gasses	Gap (evaporator) length/distance	h of evaporator	1D
[111]	Cooling of compact electronic devices	MLHP	Structural parameters of vapor groove for low and medium heat flux	FVM and mathematical model	Geometrical parameters of the groove in the evaporator	Flow and thermal transport in the evaporator	3D
[112]	Heat and mass transfer for a cylindrical evaporator of	LHP	Prestart situations when no liquid in the evaporator	Multivariant model	Heat loads and structural material of evaporator	Processes in evaporator through the first stage of startup regime	1D

Table 1 (*continued*)

Ref.	Application	Type of HP	System description	Simulation software	Input parameters (variable parameters)	Investigated Parameters	Model dimensions
	LHP under start-up operation						
[113]	Heat and mass transfer in a cylindrical evaporator of LHP with longitudinal vapor-removal grooves	LHP with a cylindrical evaporator	Heat and mass transfer in a cylindrical evaporator of heat pipe under a uniform heat supply	Mathematical formulation and finite-difference analog	Heat flux and working fluid	Temperature and pressure distribution in the evaporator	1D
[120]	Utilization of for cooling applications	MCSHP	Predicting the thermal performance of MCSHP under low mass flux and low heat flux	ε-NTU method	air flow rate, FR, and height difference	Thermal characteristics of MCSHP	1D
[121]	Telecommunication industry in China	MCSHP	Two-phase flow and heat and mass and heat transfer characteristics in MCSHP	ANSYS Fluent using different multiphase models-based Euler-Euler approach	FR	Outlet temperature, cooling capacity, and wall temperature	2D
[123]	Two-phase flow behavior of ammonia boiling in evaporator	SHP	Thermal performance of flow boiling in pipes	VOF and pressure-implicit with the splitting of operators (PISO) approach	Pipe length and diameter and mass flux	Boiling flow behavior in evaporator and h	3D
[125]	Discrete heat sources in electronic components cooling	Cylindrical HP	Simulation of nanoparticles in cylindrical HPs with separated heat sources	Fortran, tridiagonal matrix algorithm (TDMA) technique, and SIMPLE procedure	Heat load and volume fraction of nanoparticle	Thermal performance of temperature, fluid flow of velocity fields, and pressure drop	2D
[126]	Mass flow rate per radian	Cylindrical HP	Steady laminar flow and incompressible gas flow in evaporator	FVM, iterative segregated method, and SIMPLEC algorithm	Radial velocity direction	Outer wall temperature in the axial direction, R_{th}, centerline pressure, centerline velocity, and velocity vector	3D
[131]	Light emitting diode (LED) with high power	MHP	Miniature sintered heat pipe	Icepak	Fin geometries	System level heat and temperature distributions	1D
[132]	Electronic components	LHP	Ejector-assisted LHP to cool electronic devices	FORTRAN	Wick thickness, condenser length, cooling water inlet temperature, vapor line inner diameter, and mass flow rate	Performance of ELHP	1D
[168]	Cooling of PV modules	PHP	PHP for solar PV cooling	Transient numerical simulation	Tilt angle and FR	Surface temperature and thermal performance	3D
[133]	Electronic components	Finned U-shape heat pipe	Finned U-shape HP used for cooling of PC—CPU	ANSYS 10	Air velocity, heat pipe orientation, and power input	Temperature distribution	3D
[137]	HVAC	HPHE	Addition of HPHE to HVAC systems	FORTRAN and TRNSYS	Number of HPHE added to the AC system	Energy consumption and, power savings	1D
[138]	HVAC	PCHP	Models of heat transfer and energy consumption for PCHP	MATLAB R2014a and ε − NTU model	Thickness of pad, ambient temperature, RH, and air rate of pre-cooled HP	Cooling performance and energy efficiency ratio	1D
[139]	HVAC	SHP	SHP heat exchanger for AC purposes in telecommunication base stations	DeST and ε-NTU method	Rated power, Rated cooling capacity, different climate conditions, and different systems	Indoor air temperature and energy consumption	1D
[140]	Telecommuni-cation stations	MCSHP	Cooling device for stations of telecommunication	MATLAB R2007a and effectiveness-NTU method	Geometrical design and environmental conditions	Thermal performance	1D
[141]	Greenhouse	CHP	Heat pipe system for greenhouse heating	Modeling and simulation	Maximum height and heating power required	Air and soil temperature (thermal performance)	1D
[142]	HVAC	HPHE	HPHE for reducing the energy consumption of HVAC system	TRNSYS	Effect of HPHE on the existing system	Air states and meteorological year energy consumption	1D
[143]	Nuclear spent fuel pool in nuclear reactors	Wickless-heat pipe	Straight, vertical, wickless HP as a passive cooling system on the spent fuel pool	RELAP5/MOD3.2 simulation model	Initial pressure, FR of the evaporator, and its heat load, and flow rate of the water jacket	Heat transfer phenomena and heat pipe thermal performance	na
[145]	Nuclear reactors	HPHE	HPHE applied for residual heat removal systems to discharge heat from the reactor core of nuclear power plant	RNG k-ε turbulence model using SIMPLE algorithm	Velocity, pipe bundles arrangement, rows number in the fluid flow direction	Turbulence and heat transfer	3D

Table 1 (*continued*)

Ref.	Application	Type of HP	System description	Simulation software	Input parameters (variable parameters)	Investigated Parameters	Model dimensions
[146]	Nuclear reactors	Non-conventional heat pipes (square tube)	High temperature sodium heat pipes as a heat transfer device in compact high temperature reactor	FEM	Evaporator length	Vapor core, vapor pressure and velocity through the mesh wick, and wall temperatures	3D
[147]	Nuclear reactors	SHP	Large-scale HP used for cooling of spent fuel pool	Steady-state numerical model	Working fluid, heat source temperature, connection pipe length	Thermal performance	1D
[163]	Solar PV/T system	Flat HP	HP PV/T system with circulation tank and PV/T collector	TRNSYS	Circulation tank volume and tilt angle/ orientation of heat pipe PV/T system	Hourly and overall thermal and electrical performance	1D
[164]	Solar water heater system	LHP	Hybrid PV solar assisted LHP/heat pump water heater	Heat transfer resistance model, numerical simulation	Weather conditions, year-round operating characteristics, solar irradiation, and ambient air temperature	Performance of HP mode and LHP/HP hybrid mode	na
[165]	Solar collector	MCHP	Solar collector with MCHP	ANSYS fluent 15	Evaporator temperature and tilt angle	Temperature distribution and thermal conductivity	3D
[166]	Water-type photovoltaic/ thermal system	HP	HP PV/T system with flat-plate collector	Finite difference method	Ambient parameters (temperature and solar radiation intensity)	Performances of HP PV/ T system including thermal and electrical performance	2D
[161]	Solar heat pipe thermoelectric generator	HP	Solar HP thermoelectric generator (SHP-TEG)	FORTRAN	Solar irradiation intensity, the temperature of cooling water, cross-section area, length, and number of thermoelements	Maximum power output and conversion efficiency	1D
[167]	Passive solar space heating system	Heat pipe	HP assisted passive solar space heating system	MATLAB	Different climates and design parameters	Performance of direct gain, indirect gain, and integrated HP solar systems	1D
[199]	Thermal energy storage	Heat pipe	HP to enhance latent heat thermal energy storage	Finite volume approach	Input/output heat transfer rates and PCM enclosure height	Axial temperature distribution, liquid fraction, and output power	2D
[189]	Thermal management in fully electric vehicle (FEV)	LHP	Implementation of LHP in the thermal control system of FEV	Octave	LHP configurations and working fluids	Thermal performance (heat dissipation)	1D

na: not available or not applicable.

oscillating/pulsating (OHP/PHPs), finned U-shape heat pipe, cylindrical heat pipe, and microchannel separate heat pipe (MCSHP) is of high priority. However, the accomplished progress on the modeling of examined types of HPs extremely limited due to the unexpected impact when concerned with a high potential of HPs and their potential benefits compared with other conventional HEs.

Extend further simulation studies on the optimization of the prevailing different types of HEs for various engineering applications under variable operating conditions considering the climatic conditions can spread these technologies faster. Application of the software for performance evaluation of long-term operation is critical and quite recommended for future work. In spite of the thermal evaluation, the exergy analysis has a significant role in the recognition of appropriateness for thermodynamic developments of HPs in various thermal applications systems, which is limited in this essential field.

The utilization of HPs for WHR is a promising solution that requires optimizing methodologies to identify the proper operating and design parameters. More studies related to limited investigated applications such as cryogenics, hydrogen production, etc., need more deeply research. Furthermore, the augmentation of thermal performance of HPs in different applications using thermoelectric generators (TEG), phase change materials (PCMs), and nanoparticles (NPs) should be investigated. Finally, comparative studies between various simulation models for a specified application of HPs are required to distinguish the most appropriate method for determining accurately the optimum conditions.

Additional experimental and numerical investigations are necessary to demonstrate the thermal transport of NPs in HPs particularly employed for different applications. In addition, more numerical implementations are compulsory to avoid the impact of NPs size on the pressure drop, nanofluids stability, sedimentation, and corrosion. The thermal behaviours of HPs due to utilizing the nano-enhanced phase change materials (NePCMs) should be examined numerically.

7. Conclusions

The present paper introduces the simulation of conventional HPs, loop heat pipes (LHPs), pulsating/oscillating heat pipes (PHPs/OHPs), and other types such as separated heat pipes (SHPs), micro/miniature heat pipes (MHPs), and cylindrical heat pipes. Several parameters had been tested and observed under different working conditions. In the present work, the accomplished achievements in the simulation of HP systems considering the operating and design parameters are comprehensively reviewed and discussed. The general background concepts of HPs, main components, and parameters influencing the system performance are studied. Furthermore, the simulation of several heat pipe-implemented systems such as cooling of electronic components, HVAC, nuclear reactors, solar energy systems, electric vehicles, waste heat recovery systems, cryogenic, etc.,were introduced.

Most of the simulations conducted were validated with experimental results which suggest that the simulation/numerical modeling is capable

of predicting the HP performance. The majority of the simulation modeling methods of HP considered the influence of different operating and design parameters such as wick, inclination angle, filling ratio, fins, the temperature gradient between the condenser and evaporator, and groves on the thermal characteristics and the pressure drop of HPs. As well, the mentioned geometrical and operating factors influencing the optimum performance of HPs in various applications are studied. It is clear that optimizing of operating and geometrical parameters of HP is crucial for different applications to guarantee efficient thermal performances with minimum cost. However, the further optimization of integrated HPs with PCMs or nanofluids is still necessary.

PHPs can be employed in systems with very low-temperature cryogenics. Besides the fundamental mechanism of heat transfer in PHPs, the boiling point temperature of the employed working fluid plays a vital role in thermal performance. So, using fluids with a very low-boiling temperature such as neon, nitrogen, hydrogen, etc., maintains efficient PHPs for cryogenic applications.

Declaration of Competing Interest

The authors declare that they have no known competing financial interests or personal relationships that could have appeared to influence the work reported in this paper.

Acknowledgements

References

[1] A.G. Olabi, M.A. Abdelkareem, Renewable energy and climate change, Renew. Sustain. Energy Rev. 158 (2022), 112111.

[2] A.G. Olabi, K. Obaideen, K. Elsaid, T. Wilberforce, E.T. Sayed, H.M. Maghrabie, M.A. Abdelkareem, Assessment of the pre-combustion carbon capture contribution into sustainable development goals SDGs using novel indicators, Renew. Sustain. Energy Rev. 153 (2022), 111710.

[3] M. Venturelli, D. Brough, M. Milani, L. Montorsi, H. Jouhara, Comprehensive numerical model for the analysis of potential heat recovery solutions in a ceramic industry, Int. J. Thermofluids 10 (2021), 100080.

[4] D. Brough, H. Jouhara, The aluminium industry: a review on state-of-the-art technologies, environmental impacts and possibilities for waste heat recovery, Int. J. Thermofluids 1-2 (2020), 100007.

[5] H. Jouhara, A. Żabnieńska-Góra, N. Khordehgah, Q. Doraghi, L. Ahmad, L. Norman, B. Axcell, L. Wrobel, S. Dai, Thermoelectric generator (TEG) technologies and applications, Int. J. Thermofluids 9 (2021), 100063.

[6] M.A. Abdelkareem, M.A. Lootah, E.T. Sayed, T. Wilberforce, H. Alawadhi, B.A. A. Yousef, A.G. Olabi, Fuel cells for carbon capture applications, Sci. Total Environ. 769 (2021), 144243.

[7] E.T. Sayed, M.A. Abdelkareem, K. Obaideen, K. Elsaid, T. Wilberforce, H. M. Maghrabie, A.G. Olabi, Progress in plant-based bioelectrochemical systems and their connection with sustainable development goals, Carbon Resour. Conversion 4 (2021) 169–183.

[8] M. Li, Y. Liu, L. Dong, C. Shen, F. Li, M. Huang, C. Ma, B. Yang, X. An, W. Sand, Recent advances on photocatalytic fuel cell for environmental applications—The marriage of photocatalysis and fuel cells, Sci. Total Environ. 668 (2019) 966–978.

[9] K. Obaideen, M.A. Abdelkareem, T. Wilberforce, K. Elsaid, E.T. Sayed, H. M. Maghrabie, A.G. Olabi, Biogas role in achievement of the sustainable development goals: evaluation, challenges, and guidelines, J. Taiwan Inst. Chem. Eng. 131 (2022), 104207.

[10] E.T. Sayed, T. Wilberforce, K. Elsaid, M.K.H. Rabaia, M.A. Abdelkareem, K.-. J. Chae, A.G. Olabi, A critical review on environmental impacts of renewable energy systems and mitigation strategies: wind, hydro, biomass and geothermal, Sci. Total Environ. 766 (2021), 144505.

[11] M.S. Nazir, A.J. Mahdi, M. Bilal, H.M. Sohail, N. Ali, H.M.N. Iqbal, Environmental impact and pollution-related challenges of renewable wind energy paradigm – A review, Sci. Total Environ. 683 (2019) 436–444.

[12] A.G. Olabi, T. Wilberforce, E.T. Sayed, K. Elsaid, S.M.A. Rahman, M. A. Abdelkareem, Geometrical effect coupled with nanofluid on heat transfer enhancement in heat exchangers, Int. J. Thermofluids 10 (2021), 100072.

[13] H.M. Maghrabie, K. Elsaid, E.T. Sayed, M.A. Abdelkareem, T. Wilberforce, M. Ramadan, A.G. Olabi, Intensification of heat exchanger performance utilizing nanofluids, Int. J. Thermofluids 10 (2021), 100071.

[14] H. Jouhara, A. Chauhan, T. Nannou, S. Almahmoud, B. Delpech, L.C. Wrobel, Heat pipe based systems-Advances and applications, Energy 128 (2017) 729–754.

[15] H. Jouhara, Heat Pipes (Gravity-Assisted and Capillary-Driven), in, Begell House Inc., New York, 2019.

[16] H. Jouhara, 4.3 heat pipes, in: I. Dincer (Ed.), Comprehensive Energy Systems, Elsevier, Oxford, 2018, pp. 70–97.

[17] N. Blet, S. Lips, V. Sartre, Heats pipes for temperature homogenization: a literature review, Appl. Therm. Eng. 118 (2017) 490–509.

[18] B. Zohuri, Heat pipe theory and modeling. Heat Pipe Design and Technology, Springer, 2016, pp. 43–166.

[19] J.K. Calautit, B.R. Hughes, A passive cooling wind catcher with heat pipe technology: CFD, wind tunnel and field-test analysis, Appl. Energy 162 (2016) 460–471.

[20] W. Zhang, D. Zhang, C. Wang, W. Tian, S. Qiu, G. Su, Conceptual design and analysis of a megawatt power level heat pipe cooled space reactor power system, Ann. Nucl. Energy 144 (2020), 107576.

[21] B. Zohuri, Chapter 1 - Heat pipe infrastructure, in: B. Zohuri (Ed.), Functionality, Advancements and Industrial Applications of Heat Pipes, Academic Press, 2020, pp. 1–45.

[22] H. Behi, M. Ghanbarpour, M. Behi, Investigation of PCM-assisted heat pipe for electronic cooling, Appl. Therm. Eng. 127 (2017) 1132–1142.

[23] T.C. Werner, Y. Yan, D. Mullen, E. Halimic, Experimental analysis of a high temperature water heat pipe for thermal storage applications, Therm. Sci. Eng. Progress 19 (2020), 100564.

[24] A. Faghri, Heat pipes: review, opportunities and challenges, Front. Heat Pipes (FHP) 5 (2014).

[25] D.A. Reay, Thermal energy storage: the role of the heat pipe in performance enhancement, Int. J. Low Carbon Technol. 10 (2015) 99–109.

[26] B. Siedel, V. Sartre, F. Lefèvre, Literature review: steady-state modelling of loop heat pipes, Appl. Therm. Eng. 75 (2015) 709–723.

[27] S. Lips, V. Sartre, F. Lefevre, S. Khandekar, J. Bonjour, Overview of heat pipe studies during the period 2010– 2015, Interfacial Phenom Heat Transf. 4 (2016).

[28] H. Behi, M. Behi, D. Karimi, J. Jaguemont, M. Ghanbarpour, M. Behnia, M. Berecibar, J. Van Mierlo, Heat pipe air-cooled thermal management system for lithium-ion batteries: high power applications, Appl. Therm. Eng. 183, Part 2 (2020), 116240.

[29] H. Jouhara, Waste Heat Recovery in Process Industries, Wiley-VCH Verlag GmbH, 2021. Retrieved from, https://www.waterstones.com/.

[30] B. Orr, A. Akbarzadeh, M. Mochizuki, R. Singh, A review of car waste heat recovery systems utilising thermoelectric generators and heat pipes, Appl. Therm. Eng. 101 (2016) 490–495.

[31] W. Zhang, C. Wang, R. Chen, W. Tian, S. Qiu, G. Su, Preliminary design and thermal analysis of a liquid metal heat pipe radiator for TOPAZ-II power system, Ann. Nucl. Energy 97 (2016) 208–220.

[32] Y.S. Jeong, K.M. Kim, I.G. Kim, I.C. Bang, Hybrid heat pipe based passive in-core cooling system for advanced nuclear power plant, Appl. Therm. Eng. 90 (2015) 609–618.

[33] A. Shafieian, M. Khiadani, A. Nosrati, A review of latest developments, progress, and applications of heat pipe solar collectors, Renew. Sustain. Energy Rev. 95 (2018) 273–304.

[34] A. Amini, J. Miller, H. Jouhara, An investigation into the use of the heat pipe technology in thermal energy storage heat exchangers, Energy 136 (2017) 163–172.

[35] S. Lohrasbi, S.Z. Miry, M. Gorji-Bandpy, D.D. Ganji, Performance enhancement of finned heat pipe assisted latent heat thermal energy storage system in the presence of nano-enhanced H_2O as phase change material, Int. J. Hydrogen Energy 42 (10) (2017) 6526–6546.

[36] J. Krishna, P. Kishore, A.B. Solomon, Heat pipe with nano enhanced-PCM for electronic cooling application, Exp. Therm Fluid Sci. 81 (2017) 84–92.

[37] W.-.W. Wang, L. Wang, Y. Cai, G.-.B. Yang, F.-.Y. Zhao, D. Liu, Q.-.H. Yu, Thermo-hydrodynamic model and parametric optimization of a novel miniature closed oscillating heat pipe with periodic expansion-constriction condensers, Int. J. Heat Mass Transf. 152 (2020), 119460.

[38] M.A. Abdelkareem, H.M. Maghrabie, A.G. Abo-Khalil, O.H.K. Adhari, E.T. Sayed, A. Radwan, K. Elsaid, T. Wilberforce, A.G. Olabi, Battery thermal management systems based on nanofluids for electric vehicles, J. Energy Storage 50 (2022), 104385.

[39] N. Putra, T. Anggoro, A. Winarta, Experimental study of heat pipe heat exchanger in hospital HVAC system for energy conservation, Int. J. Adv. Sci. Eng. Inf. Technol. 7 (2017) 871–877.

[40] E. Babu, H. Reddappa, G.G. Reddy, Effect of filling ratio on thermal performance of closed loop pulsating heat pipe, Mater. Today: Proc. 5 (10, Part 3) (2018) 22229–22236.

[41] A. Yoon, S.J. Kim, Characteristics of oscillating flow in a micro pulsating heat pipe: fundamental-mode oscillation, Int. J. Heat Mass Transf. 109 (2017) 242–253.

[42] Y. Maydanik, S. Vershinin, M. Chernysheva, Investigation of thermal characteristics of a loop heat pipe in a wide range of external conditions, Int. J. Heat Mass Transf. 147 (2020), 118967.

[43] S. Launay, V. Sartre, J. Bonjour, Parametric analysis of loop heat pipe operation: a literature review, Int. J. Therm. Sci. 46 (7) (2007) 621–636.

[44] G. Huminic, A. Huminic, I. Morjan, F. Dumitrache, Experimental study of the thermal performance of thermosyphon heat pipe using iron oxide nanoparticles, Int. J. Heat Mass Transf. 54 (1–3) (2011) 656–661.

[45] R. Law, D. Reay, A. Mustaffar, R. McGlen, C. Underwood, B. Ng, Experimental investigation into the feasibility of using a variable conductance heat pipe for controlled heat release from a phase-change material thermal store, Therm. Sci. Eng. Progress 7 (2018) 125–130.

[46] Y.H. Yau, Y. Foo, Comparative study on evaporator heat transfer characteristics of revolving heat pipes filled with R134a, R22 and R410A, Int. Commun. Heat Mass Transf. 38 (2) (2011) 202–211.

[47] Y. Cao, X. Gao, R. Li, A liquid plug moving in an annular pipe–Heat transfer analysis, Int. J. Heat Mass Transf. 139 (2019) 1065–1076.

[48] Y. Yu, G. An, L. Wang, Major applications of heat pipe and its advances coupled with sorption system: a review, Front. Energy 13 (2019) 172–184.

[49] X. Yang, Y. Yan, D. Mullen, Recent developments of lightweight, high performance heat pipes, Appl. Therm. Eng. 33-34 (2012) 1–14.

[50] A.A. Hachicha, B.A. Yousef, Z. Said, I. Rodríguez, A review study on the modeling of high-temperature solar thermal collector systems, Renew. Sustain. Energy Rev. 112 (2019) 280–298.

[51] A. Faghri, Review and advances in heat pipe science and technology, J. Heat Transf. 134 (12) (2012), 123001.

[52] S.-.F. Li, Z.-h. Liu, Parametric study of rotating heat pipe performance: a review, Renew. Sustain. Energy Rev. 117 (2020), 109482.

[53] X. Wang, L. Luo, J. Xiang, S. Zheng, S. Shittu, Z. Wang, X. Zhao, A comprehensive review on the application of nanofluid in heat pipe based on the machine learning: theory, application and prediction, Renew. Sustain. Energy Rev. 150 (2021), 111434.

[54] M.H. Ahmadi, R. Kumar, M.E.H. Assad, P.T.T. Ngo, Applications of machine learning methods in modeling various types of heat pipes: a review, J. Therm. Anal. Calorim. 146 (2021) 2333–2341.

[55] A. Shafieian, M. Khiadani, A. Nosrati, Strategies to improve the thermal performance of heat pipe solar collectors in solar systems: a review, Energy Convers. Manag. 183 (2019) 307–331.

[56] M.A. Nazari, M.H. Ahmadi, R. Ghasempour, M.B. Shafii, How to improve the thermal performance of pulsating heat pipes: a review on working fluid, Renew. Sustain. Energy Rev. 91 (2018) 630–638.

[57] B. Yan, C. Wang, L. Li, The technology of micro heat pipe cooled reactor: a review, Ann. Nucl. Energy 135 (2020), 106948.

[58] B. Delpech, M. Milani, L. Montorsi, D. Boscardin, A. Chauhan, S. Almahmoud, B. Axcell, H. Jouhara, Energy efficiency enhancement and waste heat recovery in industrial processes by means of the heat pipe technology: case of the ceramic industry, Energy 158 (2018) 656–665.

[59] A.G. Olabi, K. Elsaid, E.T. Sayed, M.S. Mahmoud, T. Wilberforce, R.J. Hassiba, M. A. Abdelkareem, Application of nanofluids for enhanced waste heat recovery: a review, Nano Energy 84 (2021), 105871.

[60] H. Jouhara, N. Khordehgah, N. Serey, S. Almahmoud, S.P. Lester, D. Machen, L. Wrobel, Applications and thermal management of rechargeable batteries for industrial applications, Energy 170 (2019) 849–861.

[61] A. Faghri, Heat Pipe Science and Technology, Global Digital Press, 2016.

[62] C. Chan, E. Siqueiros, J. Ling-Chin, M. Royapoor, A. Roskilly, Heat utilisation technologies: a critical review of heat pipes, Renew. Sustain. Energy Rev. 50 (2015) 615–627.

[63] H. Li, Z. Liu, B. Chen, W. Liu, C. Li, J. Yang, Development of biporous wicks for flat-plate loop heat pipe, Exp. Therm Fluid Sci. 37 (2012) 91–97.

[64] Y. Li, W. Zhou, J. He, Y. Yan, B. Li, Z. Zeng, Thermal performance of ultra-thin flattened heat pipes with composite wick structure, Appl. Therm. Eng. 102 (2016) 487–499.

[65] D. Mishra, T. Saravanan, G. Khanra, S. Girikumar, S. Sharma, K. Sreekumar, P. Sinha, Studies on the processing of nickel base porous wicks for capillary pumped loop for thermal management of spacecrafts, Adv. Powder Technol. 21 (6) (2010) 658–662.

[66] T. Semenic, I. Catton, Experimental study of biporous wicks for high heat flux applications, Int. J. Heat Mass Transf. 52 (21–22) (2009) 5113–5121.

[67] S.D. Garner, Heat pipes for electronics cooling applications, Electronics Cooling 2 (1996) 18–23.

[68] F. Kreith, R.F. Boehm, Heat and mass transfer, in: F. Kreith (Ed.), Mechanical Engineering Handbook, CRC Press LLC, 1999, pp. 2–279.

[69] B. Zohuri, Functionality, Advancements and Industrial Applications of Heat Pipes, Academic Press, 2020.

[70] S. Lips, V. Sartre, F. Lefevre, S. Khandekar, J. Bonjour, Overview of heat pipe studies during the period 2010–2015, Interfacial Phenomena Heat Transf 4 (1) (2016) 33–53.

[71] N.N. Babu, H. Kamath, Materials used in heat pipe, Mater. Today: Proc. 2 (4–5) (2015) 1469–1478.

[72] P. Meisel, M. Jobst, W. Lippmann, A. Hurtado, Design and manufacture of ceramic heat pipes for high temperature applications, Appl. Therm. Eng. 75 (2015) 692–699.

[73] P. Wallin, Heat Pipe, Selection of Working fluid, Project Report, MVK160 Heat and Mass Transfer, Lund, Sweden, 2012.

[74] W. Qu, Progress Works of High and Super High Temperature Heat pipes, in: Developments in Heat Transfer, IntechOpen, 2011.

[75] Y. Zhang, A. Faghri, Advances and unsolved issues in pulsating heat pipes, Heat Transf. Eng. 29 (2008) 20–44.

[76] T. Cotter, Principles and Prospects For Micro Heat Pipes, Los Alamos National Lab., NMUSA, 1984.

[77] M.A. Abdelkareem, H.M. Maghrabie, E.T. Sayed, E.-C.A. Kais, A.G. Abo-Khalil, M. A. Radi, A. Baroutaji, A.G. Olabi, Heat pipe-based waste heat recovery systems: background and applications, Therm. Sci. Eng. Progress 29 (2022), 101221.

[78] S. Mahjoub, A. Mahtabroshan, Numerical Simulation of a conventional heat pipe, World Acad. Sci. Eng. Technol. 39 (2008) 117–122.

[79] D. Bastakoti, H. Zhang, D. Li, W. Cai, F. Li, An overview on the developing trend of pulsating heat pipe and its performance, Appl. Therm. Eng. 141 (2018) 305–332.

[80] H. Ma, Oscillating Heat Pipes, Springer, 2015.

[81] V.S. Nikolayev, Physical principles and state-of-the-art of modeling of the pulsating heat pipe: a review, Appl. Therm. Eng. 195 (2021), 117111.

[82] S. Rittidech, P. Terdtoon, M. Murakami, P. Kamonpet, W. Jompakdee, Correlation to predict heat transfer characteristics of a closed-end oscillating heat pipe at normal operating condition, Appl. Therm. Eng. 23 (4) (2003) 497–510.

[83] K. Gi, F. Sato, S. Maezawa, Flow visualization experiment on oscillating heat pipe, in: Proc. 11th International Heat Pipe Conference, 1999, pp. 149–153.

[84] X. Zhang, Experimental study of a pulsating heat pipe using FC-72, ethanol, and water as working fluids, Exp. Heat Transf. 17 (1) (2004) 47–67.

[85] C. Dang, L. Jia, Q. Lu, Investigation on thermal design of a rack with the pulsating heat pipe for cooling CPUs, Appl. Therm. Eng. 110 (2017) 390–398.

[86] B.G. Patil, P.R. Pachghare, Pulsating heat pipe for air conditioning system: an experimental study, Int. J. Sci. Res. Dev. (2016) 1312–1315.

[87] J. Clement, X. Wang, Experimental investigation of pulsating heat pipe performance with regard to fuel cell cooling application, Appl. Therm. Eng. 50 (1) (2013) 268–274.

[88] G. Burban, V. Ayel, A. Alexandre, P. Lagonotte, Y. Bertin, C. Romestant, Experimental investigation of a pulsating heat pipe for hybrid vehicle applications, Appl. Therm. Eng. 50 (1) (2013) 94–103.

[89] M. Alhuyi Nazari, M.H. Ahmadi, R. Ghasempour, M.B. Shafii, O. Mahian, S. Kalogirou, S. Wongwises, A review on pulsating heat pipes: from solar to cryogenic applications, Appl. Energy 222 (2018) 475–484.

[90] X. Han, X. Wang, H. Zheng, X. Xu, G. Chen, Review of the development of pulsating heat pipe for heat dissipation, Renew. Sustain. Energy Rev. 59 (2016) 692–709.

[91] M. Mameli, M. Marengo, S. Zinna, Thermal simulation of a pulsating heat pipe: effects of different liquid properties on a simple geometry, Heat Transf. Eng. 33 (14) (2012) 1177–1187.

[92] I. Nekrashevych, V.S. Nikolayev, Effect of tube heat conduction on the pulsating heat pipe start-up, Appl. Therm. Eng. 117 (2017) 24–29.

[93] P. Bhramara, CFD analysis of multi turn pulsating heat pipe, Mater. Today: Proc. 4 (2, Part A) (2017) 2701–2710.

[94] Z. Lin, S. Wang, R. Shirakashi, L.W. Zhang, Simulation of a miniature oscillating heat pipe in bottom heating mode using CFD with unsteady modeling, Int. J. Heat Mass Transf. 57 (2) (2013) 642–656.

[95] R. Senjaya, T. Inoue, Oscillating heat pipe simulation considering bubble generation Part I: presentation of the model and effects of a bubble generation, Int. J. Heat Mass Transf. 60 (2013) 816–824.

[96] P. Błasiak, M. Opalski, P. Parmar, C. Czajkowski, S. Pietrowicz, The thermal—flow processes and flow pattern in a pulsating heat pipe—numerical modelling and experimental validation, Energies 14 (18) (2021), 5952.

[97] M.O.M. Hamdan, Loop Heat Pipe (LHP) Modeling and Development by Utilizing Coherent Porous Silicon (CPS) Wicks, University of Cincinnati, 2003.

[98] J. Suh, Proof of Operation in a Planar Loop Heat Pipe (LHP) Based on CPS Wick, University of Cincinnati, 2005.

[99] B. Siedel, Analysis of heat transfer and flow patterns in a loop heat pipe: modelling by analytical and numerical approaches and experimental observations, PhD thesisL'Institut, National des Sciences Appliquées de Lyon (2014).

[100] Y.F. Maydanik, Loop heat pipes, Appl. Therm. Eng. 25 (5–6) (2005) 635–657.

[101] D. Douglas, J. Ku, T. Kaya, Testing of the geoscience laser altimeter system (GLAS) prototype loop heat pipe, in: 37th Aerospace Sciences Meeting and Exhibit, 1996, p. 473.

[102] Q. Su, S. Chang, M. Song, Y. Zhao, C. Dang, An experimental study on the heat transfer performance of a loop heat pipe system with ethanol-water mixture as working fluid for aircraft anti-icing, Int. J. Heat Mass Transf. 139 (2019) 280–292.

[103] T. Shioga, Y. Mizuno, H. Nagano, Operating characteristics of a new ultra-thin loop heat pipe, Int. J. Heat Mass Transf. 151 (2020), 119436.

[104] L. Mottet, M. Prat, Numerical simulation of heat and mass transfer in bidispersed capillary structures: application to the evaporator of a loop heat pipe, Appl. Therm. Eng. 102 (2016) 770–784.

[105] Y. Zhang, J. Liu, L. Liu, H. Jiang, T. Luan, Numerical simulation and analysis of heat leakage reduction in loop heat pipe with carbon fiber capillary wick, Int. J. Therm. Sci. 146 (2019), 106100.

[106] J. Li, F. Hong, R. Xie, P. Cheng, Pore scale simulation of evaporation in a porous wick of a loop heat pipe flat evaporator using Lattice Boltzmann method, Int. Commun. Heat Mass Transf. 102 (2019) 22–33.

[107] T. Kaya, R. Pérez, C. Gregori, A. Torres, Numerical simulation of transient operation of loop heat pipes, Appl. Therm. Eng. 28 (8–9) (2008) 967–974.

[108] A.A. Pozhilov, D.K. Zaitsev, E.M. Smirnov, A.A. Smirnovsky, Numerical simulation of heat and mass transfer in a 3D model of a loop heat pipe evaporator, St. Petersburg Polytechnical University J. Phys. Math. 3 (3) (2017) 210–217.

[109] E.G. Jung, J.H. Boo, A novel analytical modeling of a loop heat pipe employing the thin-film theory: part I—modeling and simulation, Energies 12 (2) (2019), 2408.

[110] M. Nishikawara, H. Nagano, Numerical simulation of capillary evaporator with microgap in a loop heat pipe, Int. J. Therm. Sci. 102 (2016) 39–46.

[111] X. Zhang, X. Li, S. Wang, Three-dimensional simulation on heat transfer in the flat evaporator of miniature loop heat pipe, Int. J. Therm. Sci. 54 (2012) 188–198.

[112] M. Chernysheva, Y.F. Maydanik, Numerical simulation of transient heat and mass transfer in a cylindrical evaporator of a loop heat pipe, Int. J. Heat Mass Transf. 51 (17–18) (2008) 4204–4215.

[113] M. Chernysheva, Y. Maydanik, Simulation of heat and mass transfer in a cylindrical evaporator of a loop heat pipe, Int. J. Heat Mass Transf. 131 (2019) 442–449.

[114] M. Leriche, S. Harmand, M. Lippert, B. Desmet, An experimental and analytical study of a variable conductance heat pipe: application to vehicle thermal management, Appl. Therm. Eng. 38 (2012) 48–57.

[115] H. Jouhara, H. Merchant, Experimental investigation of a thermosyphon based heat exchanger used in energy efficient air handling units, Energy 39 (1) (2012) 82–89.

[116] K. Ong, M. Haider-E-Alahi, Performance of a R-134a-filled thermosyphon, Appl. Therm. Eng. 23 (18) (2003) 2373–2381.

[117] L. Vasiliev, L. Vasiliev Jr, Sorption heat pipe—a new thermal control device for space and ground application, Int. J. Heat Mass Transf. 48 (12) (2005) 2464–2472.

[118] R. Bertossi, N. Guilhem, V. Ayel, C. Romestant, Y. Bertin, Modeling of heat and mass transfer in the liquid film of rotating heat pipes, Int. J. Therm. Sci. 52 (2012) 40–49.

[119] H. Arat, O. Arslan, U. Ercetin, A. Akbulut, A comprehensive numerical investigation of unsteady-state two-phase flow in gravity assisted heat pipe enclosure, Therm. Sci. Eng. Progress 25 (2021), 100993.

[120] L. Ling, Q. Zhang, Y. Yu, Y. Wu, S. Liao, Z. Sha, Simulation of a micro channel separate heat pipe (MCSHP) under low heat flux and low mass flux, Appl. Therm. Eng. 119 (2017) 25–33.

[121] C. Yue, Q. Zhang, Z. Zhai, L. Ling, CFD simulation on the heat transfer and flow characteristics of a microchannel separate heat pipe under different filling ratios, Appl. Therm. Eng. 139 (2018) 25–34.

[122] L. Cong, H. Ying, T. Jianping, Boiling-condensation heat transfer and flow characteristics in ultrathin limited enclosed space based on numerical simulation and visualization experiment, Therm. Sci. (2021) 348. -348.

[123] Y. Kuang, W. Wang, R. Zhuan, C. Yi, Simulation of boiling flow in evaporator of separate type heat pipe with low heat flux, Ann. Nucl. Energy 75 (2015) 158–167.

[124] F. Yao, C. Yu, X. Li, C. Shen, Numerical study on the heat transfer characteristics of axially grooved heat pipe assisted by gravity, Microgravity Sci. Technol. 33 (2021) 9.

[125] P. Mashaei, M. Shahryari, H. Fazeli, S. Hosseinalipour, Numerical simulation of nanofluid application in a horizontal mesh heat pipe with multiple heat sources: a smart fluid for high efficiency thermal system, Appl. Therm. Eng. 100 (2016) 1016–1030.

[126] N. Pooyoo, S. Kumar, J. Charoensuk, A. Suksangpanomrung, Numerical simulation of cylindrical heat pipe considering non-Darcian transport for liquid flow inside wick and mass flow rate at liquid–vapor interface, Int. J. Heat Mass Transf. 70 (2014) 965–978.

[127] H.M. Maghrabie, K. Elsaid, T. Wilberforce, E.T. Sayed, M.A. Abdelkareem, A.-.G. Olabi, Applications of nanofluids in cooling of electronic components, in: A.-G. Olabi (Ed.), Encyclopedia of Smart Materials 4, Elsevier, Oxford, 2022, pp. 310–318.

[128] H.M. Maghrabie, M. Attalla, H.E. Fawaz, M. Khalil, Impingement/effusion cooling of electronic components with cross-flow, Appl. Therm. Eng. 151 (2019) 199–213.

[129] H.M. Maghrabie, M. Attalla, H.E. Fawaz, M. Khalil, Numerical investigation of heat transfer and pressure drop of in-line array of heated obstacles cooled by jet impingement in cross-flow, Alexandria Eng. J. 56 (3) (2017) 285–296.

[130] H.M. Maghrabie, M. Attalla, H.E. Fawaz, M. Khalil, Effect of jet position on cooling an array of heated obstacles, J. Therm. Sci. Eng. Appl. 10 (1) (2018), 011005.

[131] D. Li, G. Zhang, K. Pan, X. Ma, L. Liu, J. Cao, Numerical simulation on heat pipe for high power LED multi-chip module packaging, in: 2009 international conference on electronic packaging technology & high density packaging, IEEE, 2009, pp. 393–397.

[132] L. Zhu, J. Yu, Simulation of steady-state operation of an ejector-assisted loop heat pipe with a flat evaporator for application in electronic cooling, Appl. Therm. Eng. 95 (2016) 236–246.

[133] M.H. Elnaggar, M. Abdullah, M.A. Mujeebu, Experimental analysis and FEM simulation of finned U-shape multi heat pipe for desktop PC cooling, Energy Convers. Manag. 52 (8–9) (2011) 2937–2944.

[134] H.M. Maghrabie, M.A. Abdelkareem, K. Elsaid, E.T. Sayed, A. Radwan, H. Rezk, T. Wilberforce, A.G. Abo-Khalil, A.G. Olabi, A review of solar chimney for natural ventilation of residential and non-residential buildings, Sustain. Energy Technol. Assessments 52, Part B (2022) 102082.

[135] R. Sukarno, N. Putra, I.I. Hakim, F.F. Rachman, T.M.I. Mahlia, Utilizing heat pipe heat exchanger to reduce the energy consumption of airborne infection isolation hospital room HVAC system, J. Build. Eng. 35 (2021), 102116.

[136] Y. Yu, L. Wang, Solid sorption heat pipe coupled with direct air cooling technology for thermal control of rack level in internet data centers: design and numerical simulation, Int. J. Heat Mass Transf. 145 (2019), 118714.

[137] M. Ahmadzadehtalatapeh, Y. Yau, The application of heat pipe heat exchangers to improve the air quality and reduce the energy consumption of the air conditioning system in a hospital ward—A full year model simulation, Energy Build. 43 (9) (2011) 2344–2355.

[138] L. Liu, Q. Zhang, L. Ling, X. Ma, Simulation investigation on pre-cooled heat pipe (PCHP) for free cooling of high thermal density space, Int. J. Refrig. 122 (2021) 210–219.

[139] D.-d. Zhu, D. Yan, Z. Li, Modelling and applications of annual energy-using simulation module of separated heat pipe heat exchanger, Energy Build. 57 (2013) 26–33.

[140] L. Ling, Q. Zhang, Y. Yu, Y. Wu, S. Liao, Study on thermal performance of micro-channel separate heat pipe for telecommunication stations: experiment and simulation, Int. J. Refrig. 59 (2015) 198–209.

[141] J. Du, P. Bansal, B. Huang, Simulation model of a greenhouse with a heat-pipe heating system, Appl. Energy 93 (2012) 268–276.

[142] Y. Yau, The use of a double heat pipe heat exchanger system for reducing energy consumption of treating ventilation air in an operating theatre—A full year energy consumption model simulation, Energy Build. 40 (5) (2008) 917–925.

[143] M.H. Kusuma, N. Putra, A.R. Antariksawan, R.A. Koestoer, S. Widodo, S. Ismarwanti, B.T. Verlambang, Passive cooling system in a nuclear spent fuel pool using a vertical straight wickless-heat pipe, Int. J. Therm. Sci. 126 (2018) 162–171.

[144] M.H. Kusuma, N.S.D. Putra, S. Ismarwanti, S. Widodo, Simulation of wickless-heat pipe as passive cooling system in nuclear spent fuel pool using RELAP5/MOD3.2, Int. J. Adv. Sci. Eng. Inf. Technol. 7 (3) (2017) 836–842.

[145] C.-.Y. Xie, H.-.Z. Tao, W. Li, J.-.J. Cheng, Numerical simulation and experimental investigation of heat pipe heat exchanger applied in residual heat removal system, Ann. Nucl. Energy 133 (2019) 568–579.

[146] K. Panda, I. Dulera, A. Basak, Numerical simulation of high temperature sodium heat pipe for passive heat removal in nuclear reactors, Nucl. Eng. Des. 323 (2017) 376–385.

[147] Y. Kuang, C. Yi, W. Wang, Modeling and simulation of large-scale separated heat pipe with low heat flux for spent fuel pool cooling, Appl. Therm. Eng. 147 (2019) 747–755.

[148] H.M. Maghrabie, A.S.A. Mohamed, M.Salem Ahmed, Experimental investigation of a combined photovoltaic thermal system via air cooling for summer weather of Egypt, J. Therm. Sci. Eng. Appl. 12 (4) (2020), 041022.

[149] H.M. Maghrabie, K. Elsaid, E.T. Sayed, A. Radwan, A.G. Abo-Khalil, H. Rezk, M.A. Abdelkareem, A.G. Olabi, Phase change materials based on nanoparticles for enhancing the performance of solar photovoltaic panels: a review, J. Energy Storage 48 (2022), 103937.

[150] A.S.A. Mohamed, H.M. Maghrabie, Techno-economic feasibility analysis of Benban solar Park, Alexandria Eng. J. 61 (12) (2022) 12593–12607.

[151] H. Maghrabie, A. Mohamed, A. Fahmy, A.A. A.bdel Samee, Performance augmentation of PV panels using phase change material cooling technique: a review, SVU-Int. J. Eng. Sci. Appl. 2 (2) (2021) 1–13.

[152] H.M. Maghrabie, K. Elsaid, E.T. Sayed, M.A. Abdelkareem, T. Wilberforce, A.G. Olabi, Building-integrated photovoltaic/thermal (BIPVT) systems: applications and challenges, Sustain. Energy Technol. Assessments 45 (2021) 101151.

[153] H.M. Maghrabie, M.A. Abdelkareem, A.H. Al-Alami, M. Ramadan, E. Mushtaha, T. Wilberforce, A.G. Olabi, State-of-the-art technologies for building-integrated photovoltaic systems, Buildings 11 (9) (2021) 383.

[154] T. Wilberforce, A.G. Olabi, E.T. Sayed, K. Elsaid, H.M. Maghrabie, M.A. Abdelkareem, A review on zero energy buildings – Pros and cons, Energy and Built Environment, (2021).

[155] A.S.A. Mohamed, M.S. Ahmed, H.M. Maghrabie, A.G. Shahdy, Desalination process using humidification–dehumidification technique: a detailed review, Int. J. Energy Res. 45 (3) (2021) 3698–3749.

[156] T. Salameh, P.P. Kumar, A.G. Olabi, K. Obaideen, E.T. Sayed, H.M. Maghrabie, M.A. Abdelkareem, Best battery storage technologies of solar photovoltaic systems for desalination plant using the results of multi optimization algorithms and sustainable development goals, J. Energy Storage 55, Part A (2022), 105312.

[157] H. Rezk, B. Alamri, M. Aly, A. Fathy, A.G. Olabi, M.A. Abdelkareem, H.A. Ziedan, Multicriteria decision-making to determine the optimal energy management strategy of hybrid PV–diesel battery-based desalination system, Sustainability 13 (8) (2021) 4202.

[158] A. Iqbal, M.S. Mahmoud, E.T. Sayed, K. Elsaid, M.A. Abdelkareem, H. Alawadhi, A.G. Olabi, Evaluation of the nanofluid-assisted desalination through solar stills in the last decade, J. Environ. Manag. 277 (2021), 111415.

[159] A. Shafieian, M. Khiadani, A. Nosrati, Thermal performance of an evacuated tube heat pipe solar water heating system in cold season, Appl. Therm. Eng. 149 (2019) 644–657.

[160] K. Chopra, A.K. Pathak, V.V. Tyagi, A.K. Pandey, S. Anand, A. Sari, Thermal performance of phase change material integrated heat pipe evacuated tube solar collector system: an experimental assessment, Energy Convers. Manag. 203 (2020) 112205.

[161] W. He, Y. Su, S. Riffat, J. Hou, J. Ji, Parametrical analysis of the design and performance of a solar heat pipe thermoelectric generator unit, Appl. Energy 88 (12) (2011) 5083–5089.

[162] H. Li, Y. Sun, Performance optimization and benefit analyses of a photovoltaic loop heat pipe/solar assisted heat pump water heating system, Renew. Energy 134 (2019) 1240–1247.

[163] B. Zhang, J. Lv, H. Yang, T. Li, S. Ren, Performance analysis of a heat pipe PV/T system with different circulation tank capacities, Appl. Therm. Eng. 87 (2015) 89–97.

[164] N. Dai, X. Xu, S. Li, Z. Zhang, Simulation of hybrid photovoltaic solar assisted loop heat pipe/heat pump system, Appl. Sci. 7 (2) (2017) 197.

[165] G. Li, T.M. Diallo, Y.G. Akhlaghi, S. Shittu, X. Zhao, X. Ma, Y. Wang, Simulation and experiment on thermal performance of a micro-channel heat pipe under different evaporator temperatures and tilt angles, Energy 179 (2019) 549–557.

[166] P. Gang, F. Huide, Z. Tao, J. Jie, A numerical and experimental study on a heat pipe PV/T system, Sol. Energy 85 (5) (2011) 911–921.

[167] M.V. Albanese, B.S. Robinson, E.G. Brehob, M.K. Sharp, Simulated and experimental performance of a heat pipe assisted solar wall, Sol. Energy 86 (5) (2012) 1552–1562.

[168] H. Alizadeh, R. Ghasempour, M.B. Shafii, M.H. Ahmadi, W.-.M. Yan, M.A. Nazari, Numerical simulation of PV cooling by using single turn pulsating heat pipe, Int. J. Heat Mass Transf. 127, Part A (2018) 203–208.

[169] A.G. Abo-Khalil, M.A. Abdelkareem, E.T. Sayed, H.M. Maghrabie, A. Radwan, H. Rezk, A.G. Olabi, Electric vehicle impact on energy industry, policy, technical barriers, and power systems, Int. J. Thermofluids 13 (2022), 100134.

[170] H. Jouhara, N. Serey, N. Khordehgah, R. Bennett, S. Almahmoud, S.P. Lester, Investigation, development and experimental analyses of a heat pipe based battery thermal management system, Int. J.Thermofluids 1-2 (2020), 100004.

[171] A.G. Olabi, H.M. Maghrabie, O.H.K. Adhari, E.T. Sayed, B.A.A. Yousef, T. Salameh, M. Kamil, M.A. Abdelkareem, Battery thermal management systems: recent progress and challenges, Int. J. Thermofluids 15 (2022), 100171.

[172] M.A. Abdelkareem, H.M. Maghrabie, A.G. Abo-Khalil, O.H.K. Adhari, E.T. Sayed, A. Radwan, H. Rezk, H. Jouhara, A.G. Olabi, Thermal management systems based on heat pipes for batteries in EVs/HEVs, J. Energy Storage 51 (2022), 104384.

[173] H. Jouhara, B. Delpech, R. Bennett, A. Chauhan, N. Khordehgah, N. Serey, S. P. Lester, Heat pipe based battery thermal management: evaluating the potential of two novel battery pack integrations, Int. J. Thermofluids 12 (2021), 100115.

[174] A.H. Alami, H.M. Maghrabie, M.A. Abdelkareem, E.T. Sayed, Z. Yasser, T. Salameh, S.M.A. Rahman, H. Rezk, A.G. Olabi, Potential applications of phase change materials for batteries' thermal management systems in electric vehicles, J. Energy Storage 54 (2022), 105204.

[175] A.G. Olabi, T. Wilberforce, E.T. Sayed, A.G. Abo-Khalil, H.M. Maghrabie, K. Elsaid, M.A. Abdelkareem, Battery energy storage systems and SWOT (strengths, weakness, opportunities, and threats) analysis of batteries in power transmission, Energy 254, Part A (2022), 123987.

[176] H. Rezk, E.T. Sayed, H.M. Maghrabie, M.A. Abdelkareem, R.M. Ghoniem, A. G. Olabi, Fuzzy modelling and metaheuristic to minimize the temperature of lithium-ion battery for the application in electric vehicles, J. Energy Storage 50 (2022), 104552.

[177] J. Kim, J. Oh, H. Lee, Review on battery thermal management system for electric vehicles, Appl. Therm. Eng. 149 (2019) 192–212.

[178] S. Lei, Y. Shi, G. Chen, Heat-pipe based spray-cooling thermal management system for lithium-ion battery: experimental study and optimization, Int. J. Heat Mass Transf. 163 (2020), 120494.

[179] C. Wan, Thermal performance of heat pipe array in battery thermal management, Tehnički vjesnik 27 (2020) 423–428.

[180] J. Deng, F. Zhou, B. Shi, J.L. Torero, H. Qi, P. Liu, S. Ge, Z. Wang, C. Chen, Waste heat recovery, utilization and evaluation of coalfield fire applying heat pipe combined thermoelectric generator in Xinjiang, China, Energy 207 (2020), 118303.

[181] C. Zhang, Z. Xia, B. Wang, H. Gao, S. Chen, S. Zong, K. Luo, A Li-Ion battery thermal management system combining a heat pipe and thermoelectric cooler, Energies 13 (4) (2020) 841.

[182] S. Hong, X. Zhang, S. Wang, Z. Zhang, Experimental Investigation on the characters of ultra-thin loop heat pipe applied in BTMS, Energy Procedia 75 (2015) 3192–3200.

[183] J. Zhao, P. Lv, Z. Rao, Experimental study on the thermal management performance of phase change material coupled with heat pipe for cylindrical power battery pack, Exp. Therm Fluid Sci. 82 (2017) 182–188.

[184] Z.Y. Jiang, Z.G. Qu, Lithium–ion battery thermal management using heat pipe and phase change material during discharge–charge cycle: a comprehensive numerical study, Appl. Energy 242 (2019) 378–392.

[185] H. Behi, D. Karimi, M. Behi, J. Jaguemont, M. Ghanbarpour, M. Behnia, M. Berecibar, J. Van Mierlo, Thermal management analysis using heat pipe in the high current discharging of lithium-ion battery in electric vehicles, J. Energy Storage 32 (2020), 101893.

[186] J. Wang, Y. Gan, J. Liang, M. Tan, Y. Li, Sensitivity analysis of factors influencing a heat pipe-based thermal management system for a battery module with cylindrical cells, Appl. Therm. Eng. 151 (2019) 475–485.

[187] D. Dan, C. Yao, Y. Zhang, H. Zhang, Z. Zeng, X. Xu, Dynamic thermal behavior of micro heat pipe array-air cooling battery thermal management system based on thermal network model, Appl. Therm. Eng. 162 (2019), 114183.

[188] F.M. Nasir, M.Z. Abdullah, M.F.M.A. Majid, M.A. Ismail, Nanofluid-filled heat pipes in managing the temperature of EV lithium-ion batteries, J. Phys. Conf. Ser. 1349 (2019), 012123.

[189] M. Bernagozzi, S. Charmer, A. Georgoulas, I. Malavasi, N. Michè, M. Marengo, Lumped parameter network simulation of a Loop Heat Pipe for energy management systems in full electric vehicles, Appl. Therm. Eng. 141 (2018) 617–629.

[190] D. Brough, J. Ramos, B. Delpech, H. Jouhara, Development and validation of a TRNSYS type to simulate heat pipe heat exchangers in transient applications of waste heat recovery, Int. J. Thermofluids 9 (2021), 100056.

[191] A. Burlacu, G. Sosoi, R.Ş. Vizitiu, M. Bărbuță, C.D. Lăzărescu, V. Ciocan, A. A. Şerbănoiu, Energy efficient heat pipe heat exchanger for waste heat recovery in buildings, Procedia Manuf. 22 (2018) 714–721.

[192] F. Yang, X. Yuan, G. Lin, Waste heat recovery using heat pipe heat exchanger for heating automobile using exhaust gas, Appl. Therm. Eng. 23 (2003) 367–372.

[193] J.J. Fierro, C. Nieto-Londoño, A. Escudero-Atehortua, M. Giraldo, H. Jouhara, L. C. Wrobel, Techno-economic assessment of a rotary kiln shell radiation waste heat recovery system, Therm. Sci. Eng. Progress 23 (2021), 100858.

[194] S. Lin, J. Broadbent, R. McGlen, Numerical study of heat pipe application in heat recovery systems, Appl. Therm. Eng. 25 (2005) 127–133.

[195] K. Natsume, T. Mito, N. Yanagi, H. Tamura, T. Tamada, K. Shikimachi, N. Hirano, S. Nagaya, Development of cryogenic oscillating heat pipe as a new device for indirect/conduction cooled superconducting magnets, IEEE Trans. Appl. Supercond. 22 (2012), 4703904. -4703904.

[196] Z.G. Qu, G. Chen, L. Zhou, J.Y. Miao, Numerical study on the operating characteristics of cryogenic loop heat pipes based on a one-dimensional heat leak model, Energy Convers. Manag. 172 (2018) 485–496.

[197] B.P. Singh, M.D. Atrey, Numerical investigation of a nitrogen based cryogenic pulsating heat pipe, Cryogenics 115 (2021), 103246.

[198] K.R. Sagar, H.B. Naik, H.B. Mehta, Numerical study of liquid nitrogen based pulsating heat pipe for cooling superconductors, Int. J. Refrig. 122 (2021) 33–46.

[199] N. Sharifi, A. Faghri, T.L. Bergman, C.E. Andraka, Simulation of heat pipe-assisted latent heat thermal energy storage with simultaneous charging and discharging, Int. J. Heat Mass Transf. 80 (2015) 170–179.

[200] J. Ramos, A. Chong, H. Jouhara, Experimental and numerical investigation of a cross flow air-to-water heat pipe-based heat exchanger used in waste heat recovery, Int. J. Heat Mass Transf. 102 (2016) 1267–1281.

[201] J.D. Holladay, J. Hu, D.L. King, Y. Wang, An overview of hydrogen production technologies, Catal. Today 139 (2009) 244–260.

[202] B. Chen, F. Wang, Numerical simulation of heat-pipe and folded reformers for efficient hydrogen production through methane autothermal reforming, Int. J. Energy Res. 44 (2020) 10430–10441.

[203] J. Wang, J.A. Apresa, M. Weathered, A. Perez, M. Corradini, Transient safety evaluation of the heat pipe microreactor – Potential energy source for hydrogen production, Int. J. Hydrogen Energy 46 (2021) 38887–38902.

[204] M.I.M. Shatat, K. Mahkamov, Determination of rational design parameters of a multi-stage solar water desalination still using transient mathematical modelling, Renew. Energy 35 (2010) 52–61.

[205] H. Jouhara, D. Bertrand, B. Axcell, L. Montorsi, M. Venturelli, S. Almahmoud, M. Milani, L. Ahmad, A. Chauhan, Investigation on a full-scale heat pipe heat exchanger in the ceramics industry for waste heat recovery, Energy 223 (2021), 120037.

[206] T.C. Jen, G. Gutierrez, S. Eapen, G. Barber, H. Zhao, P.S. Szuba, J. Labataille, J. Manjunathaiah, Investigation of heat pipe cooling in drilling applications.: part I: preliminary numerical analysis and verification, Int. J. Mach. Tools Manuf 42 (2002) 643–652.